

---

*Research Articles: Neurobiology of Disease*

## **Is Optogenetic Activation of Vglut1-positive A $\beta$ Low-Threshold Mechanoreceptors Sufficient to Induce Tactile Allodynia in Mice after Nerve Injury?**

Alexander Chamesian<sup>1</sup>, Megumi Matsuda<sup>1</sup>, Michael Young<sup>2</sup>, Michelle Wang<sup>1</sup>, Zhi-Jun Zhang<sup>1</sup>, Di Liu<sup>1</sup>, Brielle Tobin<sup>1</sup>, Zhen-Zhong Xu<sup>1</sup>, Thomas Van de Ven<sup>1</sup> and Ru-Rong Ji<sup>1,2</sup>

<sup>1</sup>*Department of Anesthesiology, Duke University School of Medicine*

<sup>2</sup>*Department of Neurobiology, Duke University School of Medicine*

<sup>3</sup>*Medical Scientist Training Program, Duke University School of Medicine*

<https://doi.org/10.1523/JNEUROSCI.2064-18.2019>

Received: 12 August 2018

Revised: 8 May 2019

Accepted: 22 May 2019

Published: 31 May 2019

---

**Author contributions:** A.C., M.Y., Z.-J.Z., D.L., Z.-Z.X., T.V.d.V., and R.-R.J. designed research; A.C., M.M., M.Y., M.W., Z.-J.Z., D.L., and Z.-Z.X. performed research; A.C., M.M., M.Y., M.W., Z.-J.Z., D.L., B.T., and Z.-Z.X. analyzed data; A.C. wrote the first draft of the paper; A.C., M.M., M.Y., T.V.d.V., and R.-R.J. edited the paper; A.C., T.V.d.V., and R.-R.J. wrote the paper.

**Conflict of Interest:** The authors declare no competing financial interests.

We thank Yawar Qadri for critical reading of the manuscript. This study is supported in part by R01DE17794 and R01NS87988 (R.-R.J) and Congressionally Directed Medical Research Programs and the Department of Defense awards W81XWH-12-2-0129 and W81XWH-15-2-0046(TV).

Corresponding Author Email: [alexander.chamesian@duke.edu](mailto:alexander.chamesian@duke.edu)

**Cite as:** J. Neurosci 2019; 10.1523/JNEUROSCI.2064-18.2019

**Alerts:** Sign up at [www.jneurosci.org/alerts](http://www.jneurosci.org/alerts) to receive customized email alerts when the fully formatted version of this article is published.

Accepted manuscripts are peer-reviewed but have not been through the copyediting, formatting, or proofreading process.

Copyright © 2019 the authors

1 **Is Optogenetic Activation of Vglut1-positive A $\beta$  Low-Threshold**  
2 **Mechanoreceptors Sufficient to Induce Tactile Allodynia in**  
3 **Mice after Nerve Injury?**

4 Alexander Chamesian<sup>1,4</sup>, Megumi Matsuda<sup>1</sup>, Michael Young<sup>2</sup>, Michelle Wang<sup>1</sup>, Zhi-Jun Zhang<sup>1</sup>, Di Liu<sup>1</sup>,  
5 Brielle Tobin<sup>1</sup>, Zhen-Zhong Xu<sup>1</sup>, Thomas Van de Ven<sup>1</sup>, and Ru-Rong Ji<sup>1,2</sup>

6  
7 <sup>1</sup>Department of Anesthesiology, Duke University School of Medicine <sup>2</sup>Department of Neurobiology, Duke University  
8 School of Medicine, <sup>3</sup>Medical Scientist Training Program, Duke University School of Medicine <sup>4</sup>Corresponding Author  
9  
10 Corresponding Author Email: alexander.chamesian@duke.edu

## 11 Abstract

12 Mechanical allodynia is a cardinal feature of pathological pain. Recent work has  
13 demonstrated the necessity of  $A\beta$  low-threshold mechanoreceptors ( $A\beta$ -LTMRs) for  
14 mechanical allodynia-like behaviors in mice, but it remains unclear whether these neurons  
15 are sufficient to produce pain under pathological conditions. Thus, we generated a  
16 transgenic mouse in which channelrhodopsin-2 (ChR2) is conditionally expressed in  
17 Vesicular Glutamate Transporter 1 (Vglut1) sensory neurons (Vglut1-ChR2), which is a  
18 heterogeneous population of large-sized sensory neurons with features consistent with  
19 ( $A\beta$ -LTMRs). In naive male Vglut1-ChR2 mice, transdermal hindpaw photostimulation  
20 evoked withdrawal behaviors in an intensity- and frequency-dependent manner, which  
21 were abolished by local anesthetic and also selective A-fiber blockade. Surprisingly, male  
22 Vglut1-ChR2 mice did not show significant differences in light-evoked behaviors or real-  
23 time aversion after nerve injury, despite marked hypersensitivity to punctate mechanical  
24 stimuli. Thus, we conclude that optogenetic activation of cutaneous Vglut1-ChR2 neurons  
25 alone is not sufficient to produce pain-like behaviors in neuropathic mice.

26 **Significance Statement:** Mechanical allodynia, wherein innocuous touch is perceived as  
27 pain, is a common feature of pathological pain. To test the contribution of low-threshold  
28 mechanoreceptors to nerve injury-induced mechanical allodynia, we generated and  
29 characterized a new transgenic mouse (Vglut1-ChR2) to optogenetically activate cutaneous  
30 Vglut1-positive LTMRs. Using this mouse, we found that light-evoked behaviors were  
31 unchanged by nerve injury, which suggests that activation of Vglut1-positive LTMRs alone  
32 is not sufficient to produce pain. The Vglut1-ChR2 mouse will be broadly useful for the  
33 study of touch, pain and itch.

## 34 Introduction

35 Low-threshold mechanoreceptors (LTMRs) are a heterogeneous class of primary sensory  
36 neuron (PSN) that subserves the sensation of innocuous touch (Zimmerman et al., 2014).  
37 Fast-conducting, myelinated LTMRs are known as  $A\beta$ -LTMRs, and these comprise the  
38 major tactile receptors in the skin (Abraira and Ginty, 2013). In addition to touch, previous  
39 studies in humans and rodents have suggested that under pathological conditions, such as  
40 inflammation or neuropathy,  $A\beta$ -LTMRs can also mediate the sensation of pain induced by  
41 touch, a phenomenon referred to as mechanical allodynia (Torebjörk et al., 1992; Lolognier  
42 et al., 2015). For chronic pain sufferers, mechanical allodynia can be highly disabling, since  
43 the myriad tactile stimuli of daily living (e.g. clothing brushing against skin) evoke pain.

44 Despite much study, it is still unknown which type of PSN mediates mechanical allodynia.  
45 Mechanical allodynia could result from the sensitization of nociceptors such that innocuous  
46 tactile stimuli are able to activate them. Another possibility is that LTMRs, which are  
47 normally activated by innocuous tactile stimuli, could gain the ability to signal to central  
48 nociceptive circuits following an insult, giving rise to pain from touch (i.e. allodynia)

49 (Latremoliere and Woolf, 2009). To distinguish between these possibilities, it is necessary  
50 to be able to activate a single population of PSN in the context of mechanical allodynia,  
51 since a natural mechanical stimulus cannot exclusively engage a single type of sensory  
52 neuron.

53 To that end, we developed and characterized a novel transgenic mouse line, *Vglut1-ChR2*,  
54 to enable transdermal optogenetic activation of  $A\beta$ -LTMRs. We demonstrate that in the  
55 *Vglut1-ChR2* mouse, *ChR2* is expressed in the majority of  $A\beta$ -LTMRs as well as some  
56 proprioceptors but not in C- or A-nociceptors. We show that optogenetic stimulation of  
57 cutaneous *Vglut1-ChR2*  $A\beta$ -LTMRs elicits non-nociceptive paw withdrawal behaviors in  
58 naive mice and is not aversive. Surprisingly, in the setting of nerve injury-induced  
59 neuropathy, optogenetic activation of *Vglut1-ChR2* neurons does not produce pain-like  
60 behaviors such as licking, jumping or vocalization, and also does not produce aversion,  
61 suggesting that *Vglut1*-expressing  $A\beta$ -LTMRs alone may not be sufficient to produce pain,  
62 even under pathological conditions.

## 63 **Methods**

### 64 **Animals**

65 The *Slc17a7-IRES2-Cre* (*Vgut1-Cre*) mouse line was obtained from Jackson lab (023527).  
66 Details for the construction of this mouse were described in (Harris et al., 2014). The *Ai32*  
67 line, which was also from Jackson Lab (024109), possess the *ChR2(H134R)-EYFP* transgene  
68 in the *ROSA26* locus. Expression of the *ChR2-(H134R)-EYFP* is made Cre-dependent by  
69 separation of the CAG promoter from the transgene by a loxP-flanked STOP  
70 cassette (Madisen et al., 2012). Male *Vglut1-Cre* mice homozygous for the Cre allele were  
71 mated with homozygous *Ai32* mice to produce compound heterozygote offspring (*Vglut1-*  
72 *ChR2*), each bearing a Cre and *Ai32* allele. To produce control subjects for some  
73 experiments, *Vglut1-Cre* homozygotes were crossed with the *R26-EYFP* line (Srinivas et al.,  
74 2001) obtained from Jax (006148), producing compound heterozygous offspring that  
75 express EYFP in *Vglut1-Cre*-positive cells. *Nav1.8-ChR2* mice were generated by crossing  
76 *Nav1.8-Cre* (Agarwal et al., 2004) with *Ai32*. *Npy2r-ChR2* mice were generated by crossing  
77 homozygous *Npy2r-IRES-Cre* males (Chang et al., 2015), which were obtained from Jackson  
78 Lab (029285), with homozygous *Ai32* females.

### 79 **Spared Nerve Injury**

80 The spared nerve injury (SNI) model was performed as previously described (Bourquin et  
81 al., 2006). Briefly, mice were anesthetized under 2% isoflurane. An incision was made near  
82 the lower thigh region, and the tibial, common peroneal and sural nerves were exposed.  
83 The tibial and common peroneal nerves were transected using small iris scissors. Care was  
84 taken to avoid touching or stretching the sural nerve. The muscle was closely  
85 approximated, and the skin incision was closed using 9 mm wound clips (Fine Science  
86 Tools). Animals were returned to their home cages following surgery and monitored.



## 87 **Intraplantar Injections**

88 Ropivacaine (0.5%, 20  $\mu$ l) was injected subcutaneously into the ventral left hindpaw  
89 using a 29g insulin syringe. Care was taken to avoid bleeding. A mixture of QX-314 (Sigma,  
90 552233) and Flagellin (Invivogen) was prepared to a final concentration of 60 mM QX-314  
91 and 1  $\mu$ g Flagellin in sterile PBS, as described previously (Xu et al., 2015). Sterile PBS was  
92 used as vehicle. 20  $\mu$ l of each solution was injected intraplantarly in a randomized and  
93 blinded fashion (A.C.)

## 94 **Behavior**

95 Animals mice (1-4 months of age) of both sexes were used in this study. Mice were housed  
96 in the animal care facilities of Duke University School of Medicine. Animals were kept on a  
97 12h light/dark cycle. All the animal procedures were approved by the Institutional Animal  
98 Care and Use Committee of Duke University. Animal experiments were conducted in  
99 accordance with the NIH Guide for the Care and Use of Laboratory Animals.

100 Animals were habituated to the behavior testing room for at least two days before testing  
101 commenced. On each day of habituation, and on testing days, mice were placed in  
102 individual, cylindrical plexiglass containers (2.75" ID, 3" Height) with a mesh floor (1/4" x  
103 1/4" in) and allowed to habituate for at least 2 hours. Behavioral testing occurred between  
104 11AM - 6PM.

## 105 **Mechanical Threshold**

106 Mechanical thresholds were assayed using calibrated von Frey filaments (North Coast  
107 Medical) and the Simplified Up-Down Method (SUDO) (Bonin et al., 2014). Fibers were  
108 applied to the sural territory of the hindpaw. Thresholds were determined first for the  
109 ipsilateral paw (left) for all mice, and then the contralateral (right) for all mice.

## 110 **Optogenetic Stimulation**

111 A 470 nm LED (Thor Labs, M470F3) was coupled to a 1000  $\mu$ m fiber (Prizmatix) and an  
112 LED driver (D2200, Thor Labs) was used to control the stimulus parameters. For all  
113 experiments, 5 ms pulse widths were used. Frequency was varied between 2-10Hz, as  
114 indicated. Light intensity was varied between 1-10  $mw/mm^2$  as indicated in each  
115 experiment. Light intensity was measured at the tip using a power meter (PM100D, Thor  
116 Labs.) All behavior was recorded for later analysis using a smartphone camera (iPhone 6S)  
117 at 30 frames per second (fps). For plantar photostimulation, the LED-coupled fiber was  
118 brought into close proximity (1-2 mm) of the plantar hindpaw but without touching.  
119 Stimulation was carried out for 10s, which was counted as a trial. For behavior in Fig. 6, for  
120 each mouse, 3 trials per mouse were performed, alternating between paws, with at least 2  
121 minutes between trials. Frequency was increased sequentially from 2Hz to 5Hz and then 10  
122 Hz. At each frequency, the intensity was also varied at 1, 2.5, 5 and 10  $mw/mm^2$ . For the  
123 experiment in Fig. 7, 2 Hz was used for all intensities in order to accurately measure single  
124 events. For the experiment depicted in Fig. 8, 5  $mw/mm^2$  and 10 Hz was used. For the

125 experiment depicted in Fig.9-10,  $10\text{ mw/mm}^2$ , 10 Hz was used. We selected this  
126 stimulation setting because it most reliably produced light-evoked behaviors.

### 127 Behavior Scoring and Analysis

128 Behaviors were scored from recorded videos using either an iPhone 6S (Apple) or Logitech  
129 HD Pro Webcam C920 (Logitech) acquired at the time of testing. Behavioral coding was  
130 conducted using the open source event-logging software BORIS (Friard and Gamba, 2016).  
131 The following ethogram was used:

132 Lift: Rapid up and down movement, Hold: Paw pulled upward toward the bottom and held  
133 Flutter: Rapid, repeated lifts in succession, Jump: Both hindpaws come off the floor, Lick:  
134 Paw moved to the mouth and licked, Guard: Paw lifted and held laterally and at mid-body  
135 level, Vocalization: Audible sound such as a squeak, Rear: Mouse extends body vertically  
136 and stands on hind legs with support of enclosure.

137 For the A-fiber blockade experiment depicted in Fig.8B-C, and the SNI experiments  
138 depicted in Fig.10, both the tester (AC) and the scorer (MM) were blind to treatment.

139 Behaviors were classified as reflexive or affective-motivational in accordance with the  
140 definitions in Corder *et al.* (Corder et al., 2017):

141 Withdrawal reflexes: rapid reflexive retraction of the paw that occurs in response to  
142 nociceptive sensory information, but ceases once the stimulus is removed and afferent  
143 nociceptive information stops.

144

145 Affective-motivational responses: temporally delayed (relative to the noxious stimulus  
146 contact or removal of said stimulus), directed licking and biting of the paw (termed  
147 'attending'), extended lifting or guarding of the paw and/or escape responses characterized  
148 by hyperlocomotion, rearing or jumping away from the noxious stimulus.

149 In this study, we classified lifting, holding and flutter as withdrawal reflexes and licking,  
150 vocalization, rearing, jumping and guarding as affective-motivational responses.

151 Exported data from BORIS was further analyzed in R. Plotting and statistical analysis were  
152 performed using the following packages: tidyverse, cowplot, readxl, colorblindr,  
153 viridis, lme, lsmeans.

### 154 Real-Time Place Escape Avoidance

155 A custom two-chamber apparatus was fashioned with each chamber having dimensions of  
156 10cm x 10cm x 15cm and white, opaque walls. A 5 cm x 4 cm hole was made at the  
157 midpoint of the wall joining the two chambers. Horizontal black striped walls were present  
158 in one chamber, and vertical stripes in the other in order to provide visually distinct cues  
159 for each chamber. The two-chamber apparatus was positioned on top of the same mesh  
160 floor used for other behavior experiments. A camera (Logitech HD Pro Webcam C90) was  
161 positioned above the chambers. Real-time tracking automated video tracking was carried  
162 out by a connected PC (Dell) running the ANY-MAZE (Stoelting) tracking software.

163 A mouse was introduced into one of the two chambers at random. Mice were first allowed  
164 to freely explore two chambers for 10 mins (Pre-stimulation). During this Pre period, the  
165 majority of mice exhibited a preference for one or the other chamber. The chamber in  
166 which each mouse spent the majority of the pre-stimulation period was taken as its  
167 preferred chamber. Immediately following the pre-stimulation period, the stimulation  
168 period (Stim) was commenced, during which time each mouse was allowed to move freely  
169 between chambers. Whenever the mouse was in its preferred chamber, blue light (470 nm,  
170 10  $mw/mm^2$ , 10Hz) was applied to a single hindpaw (left), and whenever the mouse was  
171 in its non-preferred chamber, off-spectrum, yellow light (565 nm) was applied to the  
172 hindpaw with a fiber-coupled LED (Thor Labs, M565F1) 10  $mw/mm^2$  in order to control  
173 for the presence of an experimenter and visual stimulation from light application. After the  
174 10 minute stimulation period, light application ceased, and the mice were allowed to move  
175 freely between chambers during a 10 minute post-stimulation (Post) period. For the RT-  
176 PEA assay depicted in Fig.10, mice were stimulated with blue light on the ipsilateral (left)  
177 paw when in the preferred chamber, and on the contralateral paw when in the non-  
178 preferred chamber, analogous to the traditional RT-PEA assay performed with von Frey  
179 fibers<sup>34</sup>.

#### 180 Immunohistochemistry and *In situ* hybridization

181 Animals were deeply anesthetized with isoflurane and transcardially perfused with 4%  
182 paraformaldehyde. After perfusion, lumbar DRG (L3-L5) and spinal cord were removed  
183 and postfixed in the same fixative for 2h at 4°C. Then, the tissues were cryopreserved in  
184 30% sucrose/PBS solution for at least 24 hours. All tissues were mounted in Optimal  
185 Cutting Temperature (OCT) medium (Tissue-Tek) or PBS (free-floating sections) and  
186 cryosectioned using a cryostat (Leica). For immunofluorescence and *in situ* hybridization,  
187 DRG sections were cut at 12  $\mu m$  and thaw-mounted onto Superfrost Plus slides (VWR), and  
188 spinal cord sections were cut at 14  $\mu m$  and thaw-mounted.

189 For immunostaining of DRG, sections were blocked in a solution containing 1% BSA and  
190 0.4% Triton-X 100 for 1 h at room temperature (RT). After blocking, the sections were then  
191 incubated overnight with primary antibodies diluted in 1% BSA with 0.2% Triton-X 100 at  
192 4°C. After washing 3 times in PBS for 5 minutes at RT, sections were incubated with the  
193 appropriate secondary antibody for 1 h at RT followed by 3 washes in PBS for 5 minutes.  
194 Before mounting, some sections were counterstained with DAPI and fluorescent Nissl stain  
195 (NeuroTrace 640/660, Thermo Fisher Scientific). Slides were then mounted in Prolong  
196 Gold (Life Technologies) and allowed to dry overnight at room temperature.

197 *In situ* hybridization was performed using the RNAscope system (Advanced Cell  
198 Diagnostics) according to the manufacturer's recommendations. Tissue pretreatment for  
199 DRG sections consisted of incubation with protease IV for 30 minutes at room temperature.  
200 Subsequently, the protocol for the Multiplex Fluorescent Kit v2 was followed without  
201 modification until the final wash step, after which immunostaining with anti-GFP antibody  
202 was performed. Combining immunostaining with RNAscope was necessary to recover the  
203 Chr2-EYFP signal, since the protease treatment abolishes the native EYFP fluorescence.  
204 Probes for Slc17a7 (Mm-Slc17a7, 416631), Ret (Mm-Ret, 431791), Tlr5 (Mm-Tlr5,  
205 451601), Ntrk2 (Mm-Ntrk2-C2, 423611-C2), and Nefh (Mm-Nefh-C3, 443671-C3).

206 Skin immunostaining was performed as in as described by Arcourt *et al.* Briefly, skin from  
207 the hindpaw was first fixed in methanol/acetone (1:1) for 30 mins at  $-20^{\circ}\text{C}$ , washed four  
208 times with PBS, and then incubated in 30% sucrose for at least 24 hours at  $4^{\circ}\text{C}$ . After  
209 embedding in OCT,  $50\mu\text{m}$  cryosections were cut, dried, incubated in 50mM Glycine for  
210 45min, washed twice with PBST (0.2%), blocked 1h with blocking buffer (PBST  
211 (0.2%),10% horse serum,1% BSA) and then incubated with primary antibodies overnight  
212 at  $4^{\circ}\text{C}$ . After primary staining, sections were washed three times, incubated with secondary  
213 antibody at room temperature for 1h, washed three times, counterstained with DAPI and  
214 then mounted with Prolong Gold.

215 Primary antibodies were used at the following dilutions: mouse anti-NF200 (1:500, Sigma,  
216 N0142, RRID:AB\_477257), chicken anti-GFP (1:1000, Abcam, 13970, RRID:AB\_300798),  
217 anti-CGRP (1:1000, Sigma C8198,RRID:AB\_259091), rabbit anti-TH (1:1000, Millipore  
218 AB152,RRID:AB\_390204), TROMA-1 (Iowa Developmental Studies Hybridoma Bank,  
219 1:200). Secondary antibodies were as follows: Cy3-conjugated anti-Rabbit IgG (1:500,  
220 Jackson ImmunoResearch), Alexa 488-conjugated anti-Chicken IgG (1:500, Jackson  
221 ImmunoResearch), Alexa 546-conjugated anti-Chicken IgG (1:500, Thermo Fisher  
222 Scientific), Cy3-conjugated anti-Mouse IgG (1:500, Jackson ImmunoResearch). For some  
223 sections, Alexa 568-Isolectin GS-IB4 from Griffonia simplicifolia (Thermo Fisher Scientific)  
224 was used at a 1:1000 dilution during secondary antibody incubation.

## 225 **Image Analysis**

226 Imaging was performed using an epifluorescence microscope (Nikon Eclipse NiE). For  
227 quantification, all images were taken using the same acquisition settings. For DRG  
228 quantitation, every fifth section was counted, with 2-4 DRG sections from each animal.  
229 Images in Fig.1 were analyzed in Adobe Photoshop CC. For each staining combination, a  
230 threshold was set and globally applied for each color channel and co-expression events  
231 were counted manually. For ISH experiments in Fig.2, we used the bioimage analysis  
232 software QuPath (Bankhead et al., 2017). Borders were drawn manually around cells to  
233 define regions of interest. The cross-sectional area and mean intensity for each color  
234 channel were extracted for each cell. A histogram of the mean intensities for each channel  
235 was plotted in R. For Chr2-EYFP a clear bimodal distribution was apparent, and the  
236 boundary between the population was used to classify cells as positive or negative. For *Ret*  
237 and *Nefh* a continuous distribution was apparent. To set a threshold for each channel, we  
238 sampled cells in QuPath that were judged to be completely negative of signal, and we set a  
239 threshold one standard deviation above the mean of the negative cells. Cells above the  
240 threshold were considered positive. The areas of the cells from this set were used to  
241 determine the proportion of Chr2-EYFP cells comprising each size class in Fig. 1D. *Tlr5* was  
242 expressed more sparsely and presented as puncta rather than filling the whole cell. Thus,  
243 we used instead the 'subcellular detection' analysis feature of QuPath to count individual  
244 spots. A spot threshold was set and cells with spot counts above the threshold were  
245 classified as positive.

## 246 Patch Clamp Recordings in Dissociated DRG Neurons

247 DRGs were aseptically removed from mice (5-6 weeks old) and digested with collagenase  
248 Type II (0.2 mg/mL Roche) and Dispase II (3 mg/mL Worthington) for 120 min. Cells were  
249 seeded onto poly-D-lysine coated glass coverslips and incubated for 16-48 hrs in  
250 Neurobasal (10% FBS, 2% B27, and 1% Antibiotic-Antimycotic) at 37°C with 5% CO<sub>2</sub> prior  
251 to the experiment. Whole-cell voltage clamp recordings were performed at room  
252 temperature with an EPC10 amplifier (HEKA). Pipettes were pulled from borosilicate glass  
253 to a resistance of 2-5 M $\Omega$ . The bath solution consisted of 140 mM NaCl, 3 mM KCl, 2 mM  
254 MgCl<sub>2</sub>, 2 mM CaCl<sub>2</sub>, 10 mM glucose, and 10 mM HEPES. The internal pipette solution  
255 consisted of 5 mM NaCl, 130 mM K-gluconate, 2 mM MgCl<sub>2</sub>, 10 mM EGTA, and 10 mM  
256 HEPES. Optical stimulations were performed using 470 nm light delivered from a 40x  
257 objective (Olympus). The light source was white light (CoolLED pE-300) filtered with a GFP  
258 Fluorecence Cube Set (470/525 Em/Ex) at 10% maximum intensity. Series resistance was  
259 compensated at least 60% and only cells for which the resistance remained stable and  
260 below M $\Omega$  were used for subsequent analysis. Liquid junction potential, calculated using  
261 the JPCalc software, was corrected post hoc. Analysis of the spike success rate was  
262 performed following a 5s optogenetic stimulation at 5 or 10 Hz. This was repeated 5 times  
263 per cell with 10s in between stimulus bouts. The corresponding activity was binned at the  
264 appropriate period associated with the stimulus frequency and the mean success rate was  
265 calculated as a function of pulse number across cells. The shaded region signifies the  
266 standard error of the mean.

## 267 Experimental Design and Statistical Analyses

268 Behavioral tests were conducted in a blinded fashion both during data acquisition and  
269 scoring, with the exception of the experiments presented in Figures 6-7, where the tester  
270 (AC) was aware of the identity of the subjects. The scorers (MM, BT) were blind to the  
271 identity of the subjects, however, during scoring. Scoring of behavioral data was performed  
272 in a blinded fashion after data acquisition using the open source behavioral coding  
273 software BORIS or automatically by video analysis (RT-PEA). Imaging data acquisition was  
274 performed by an investigator with knowledge of the identity of the experimental groups  
275 (MW, AC, MM). Statistical tests for behavioral experiments where subjects were repeatedly  
276 measured consisted of factorial linear mixed effects (LME) models with subject as a  
277 random effect. Test results for each behavioral experiment are indicated in the figure  
278 caption. Statistical tests were conducted in R (<http://www.R-project.org/>). Group sizes for  
279 behavioral, imaging and electrophysiological experiments were based on previous such  
280 experiments in our lab.

281



## 282 Results

### 283 Distribution of ChR2-EYFP in the Dorsal Root Ganglia

284 To gain genetic access to A $\beta$ -LTMRs, we crossed a Vglut1-Cre transgenic mouse line  
285 (Slc17a7-IRES2-Cre) (Harris et al., 2014) to a Cre-dependent ChR2-EYFP reporter line  
286 (Ai32) (Madisen et al., 2010) because it has been demonstrated that Vglut1 is expressed  
287 preferentially in low-threshold mechanoreceptors (Alvarez et al., 2004; Brumovsky et al.,  
288 2007), in contrast to *Vglut2* and *Vglut3*, which are expressed preferentially by nociceptors  
289 and C-fiber LTMRs, respectively (Rogoz et al., 2012). We refer to the offspring of this cross  
290 as Vglut1-ChR2.

291 To examine the distribution of ChR2-EYFP and co-expression with canonical class markers,  
292 we performed immunohistochemical staining and *in situ hybridization* on lumbar DRGs of  
293 Vglut1-ChR2 mice (Fig. 1A-C). Fourteen percent (14%, 248/1667) of all DRG neurons (Nissl  
294 Stain) expressed ChR2-EYFP. Ninety-five (95%, 487/505 neurons) percent of ChR2-EYFP-  
295 positive neurons in Vglut1-ChR2 mice co-expressed *Vglut1* mRNA by *in situ* hybridization,  
296 while fifty-nine percent (59%, 487/830 neurons) of *Vglut1*-positive neurons co-expressed  
297 ChR2-EYFP, demonstrating that ChR2-EYFP expression is highly specific but incompletely  
298 penetrant.

299 Seventy-eight percent (78%, 228/296 neurons) of ChR2-EYFP-positive neurons co-  
300 expressed NF200, a marker of myelinated fibers (Berta et al., 2017). Conversely, forty-two  
301 percent (42%, 228/561 neurons) of NF200-positive neurons co-expressed ChR2-EYFP.  
302 ChR2-EYFP-positive neurons showed negligible co-expression with isolectin-B4 (IB4, 3%,  
303 10/351 neurons) and calcitonin gene-related peptide (CGRP, 5%, 13/263), markers of non-  
304 peptidergic and peptidergic nociceptors, respectively (da Silva Serra et al., 2016). Co-  
305 expression of ChR2-EYFP-positive neurons with tyrosine hydroxylase (TH), a marker of  
306 low-threshold, unmyelinated C-LTMRs (Draxler et al., 2014), was virtually undetectable  
307 (2%, 5/229 neurons). Overall, the mean cross-sectional area of ChR2-EYFP-positive  
308 neurons ( $786 \pm 20 \mu\text{m}^2$ , n=248), was substantially larger than that of all DRG neurons  
309 ( $368 \pm 6 \mu\text{m}^2$ , n=1667) (Fig. 1D). Consistently, we also found that ChR2-EYFP-positive  
310 neurons constituted more than half of all large-sized neurons ( $> 600 \mu\text{m}^2$ ) (Fig. 1E). Taken  
311 together, these results indicate that vast majority of ChR2-EYFP-positive cells in Vglut1-  
312 ChR2 mice are myelinated, medium- to large-sized neurons that express *Vglut1* and are not  
313 nociceptors or C-LTMRs.

314 To further characterize the identities of Vglut1-ChR2 neurons, we used *in situ* hybridization  
315 to determine the co-expression of ChR2-EYFP with more specific markers of A $\beta$ -LTMRs,  
316 *Ret* and Toll-Like Receptor 5 (*Tlr5*) (Fig 2A-B). *Ret* is a marker for rapidly-adapting A $\beta$ -  
317 LTMRs (A $\beta$  RA-LTMRs) (Luo et al., 2009), A $\beta$ -field LTMRs (Bai et al., 2015) as well as non-  
318 peptidergic C-nociceptors. To distinguish between LTMRs and C-nociceptors, we used the  
319 combination of *Ret* with *Nefh* (i.e. mRNA for NF200) to identify *Ret*-expressing A $\beta$ -LTMRs.  
320 *Tlr5* is expressed broadly by A $\beta$ -LTMRs but not other types of PSN (Xu et al., 2015). A large  
321 portion of the ChR2-EYFP-positive population (35%, 180/532) co-expressed the  
322 combination of *Ret/Nefh*, indicating that these are either A $\beta$  RA- or field-LTMRs. A

323 comparable fraction of all *Ret/Nefh* neurons (41%, 180/428) co-expressed ChR2-EYFP  
324 (Fig. 2C-D). More than half of all ChR2-EYFP-positive neurons co-expressed *Tlr5* (66%,  
325 340/541), and (42%, 340/800) of *Tlr5*-positive neurons co-expressed ChR2-EYFP (Fig. 2E),  
326 further corroborating the identification of these neurons as  $A\beta$ -LTMRs. Additionally, we  
327 examined the expression of *TrkB* by ISH, as this gene is known to mark  $A\beta$ -RA-LTMRs and  
328  $A\delta$ -LTMRs (Bourane et al., 2009). Interestingly, we found that most neurons expressing  
329 high levels of *TrkB* do not co-express ChR2-EYFP, but some ChR2-EYFP do express low  
330 levels of *TrkB*, as do satellite glia (Fig. 3)

331

### 332 **Spinal and cutaneous projections of Vglut1-ChR2 DRG neurons**

333 In the spinal cord, ChR2-EYFP-positive afferent fibers were evident in the deep dorsal horn  
334 (lamina III-lamina V), the dorsal columns (DC), and to a lesser extent, the ventral horn (Fig.  
335 4A). ChR2-EYFP-positive fibers were not present in the superficial laminae (I-III), where  
336 most nociceptive inputs are processed (Basbaum et al., 2009), as evidenced by the lack of  
337 overlap with CGRP-positive or IB4-positive afferents. The absence of ChR2-EYFP-positive  
338 fibers in the superficial dorsal horn suggests that they are not C- or  $A\delta$ -nociceptors. The  
339 high density of ChR2-EYFP-positive afferents in the deep laminae and dorsal columns  
340 supports the identification of the remainder of the afferents in this region as  $A\beta$ -LTMRs.  
341 The presence of ChR2-EYFP-positive fibers in the ventral horn also indicates that some  
342 ChR2-EYFP-positive neurons are proprioceptors, consistent with previous findings  
343 regarding Vglut1 expression in the spinal cord (Todd et al., 2003).

344 In the skin, ChR2-EYFP-positive afferents were present in the dermis and formed  
345 characteristic cutaneous end organs. In the glabrous skin of the hindpaw, ChR2-EYFP-  
346 positive fibers were present in close contact with TROMA1-positive Merkel cells in Merkel  
347 cell-neurite complexes (Fig 4B-Top), and also in Meissner corpuscles in the dermal  
348 papillae (Fig 4B-Middle), which are features of slowly-adapting (SA) and rapidly-adapting  
349 (RA)  $A\beta$ -LTMRs, respectively (Abraira and Ginty, 2013). In the hairy skin of the hindpaw,  
350 ChR2-EYFP-positive fibers were also found encircling hair follicles in longitudinal  
351 lanceolate endings<sup>24</sup>. These findings demonstrate that the population of cutaneous ChR2-  
352 EYFP-positive fibers represents at least two distinct subtypes of  $A\beta$ -LTMR.

### 353 **Electrophysiological characterization of Vglut1-ChR2 DRG Neurons**

354 Patch clamp recording was performed on dissociated DRG neurons from *Vglut1-ChR2* mice  
355 *in vitro*. The majority of ChR2-YFP-positive neurons (6/7) responded with only a single or a  
356 few spikes after receiving constant photostimulation (1s), followed by a prolonged  
357 depolarization above baseline which was absent in ChR2-EYFP-negative controls (Fig. 5A,  
358 H). The majority of ChR2-EYFP-positive DRG neurons faithfully produced action potentials  
359 up to a stimulus frequency of 10 Hz whereas ChR2-EYFP-negative DRG neurons did not.  
360 This suggests the neuronal activity was entrained to the stimulus specifically in the subset  
361 of DRG neurons expressing ChR2-EYFP. (Fig. 5B-D). ChR2-EYFP-positive DRG neurons all  
362 lacked an inflection in the repolarization phase often found in ChR2-EYFP-negative  
363 neurons (Fig. 5E). Further characterization of the spike waveform revealed that the width  
364 at half-maximal activation of ChR2-EYFP-positive DRG neurons was significantly lower



365 than that of ChR2-EYFP-negative neurons (Fig. 5F). Both of these properties are consistent  
366 with those of LTMRs (Ewan St John Smith, 2009). Spike thresholds, were also found to be  
367 significantly lower in ChR2-EYFP-positive DRG compared to ChR2-EYFP-negative neurons  
368 (Fig. 5E)

369

370

### 371 **Light-evoked withdrawal behaviors in naive Vglut1-ChR2 mice**

372 We applied blue light (470nm) to the plantar surface of the hindpaw to assess the  
373 behavioral response to activation of Vglut1-ChR2 neurons. We measured several facets of  
374 the behavioral response. We took paw withdrawal as a primary measure but we also  
375 measured secondary behaviors that reflect the nature of the withdrawal. We classified  
376 behaviors as “Reflexive” (Lift, Hold, Jump, Flutter) and others as “Affective-Motivational”  
377 (Guard, Lick, Rear, Vocalize) in accordance with the paradigm described in Corder *et al*  
378 (Corder et al., 2017). A full description of the scoring paradigm can be found in the  
379 Methods. We also scanned a range of light intensities (1-10  $mW/mm^2$ ) and frequencies (2-  
380 10Hz) consistent with the parameters used in similar studies of optogenetic stimulation of  
381 primary sensory neurons (Arcourt et al., 2017).

382 The typical response to photostimulation of the hindpaw was a rapid paw lift or no  
383 response, depending on the stimulation parameters. Response frequency, which measures  
384 whether the mouse responded at all during a 10s trial, increased with both light intensity  
385 and frequency (Fig. 6A), reaching maximum at 10  $mw/mm^2$ . The total number of events  
386 per trial also increased with increasing intensity and frequency (Fig. 6B). At all intensities  
387 and frequencies, the most frequently observed behavior was lifting (Fig. 6C). Affective-  
388 motivational behaviors were scarcely seen, even at the highest intensities and frequencies  
389 while reflexive behaviors increased up to 10  $mw/mm^2$  (Fig. 6D-E).

390

391

392

393 To better understand the nature of the light-evoked responses in Vglut1-ChR2 mice, we  
394 directly compared paw withdrawal behaviors in Vglut1-ChR2 mice to those of Nav1.8-ChR2  
395 mice, a line which conditionally expresses ChR2 in the majority of nociceptors and has been  
396 thoroughly characterized previously (Daou et al., 2013) . For this comparison, we used low  
397 frequency (2Hz) so that we could accurately measure individual events. The response  
398 frequency of Nav1.8-ChR2 was significantly greater than that of Vglut1-ChR2 at 1  $mw/mm^2$   
399 and 2.5  $mw/mm^2$  (Fig. 7A). The number of behavioral responses per trial was markedly  
400 different between the two mouse lines; Nav1.8-ChR2 mice responded to light many more  
401 times during a 10s trial than did Vglut1-ChR2 mice at every intensity (Fig. 7B). In contrast  
402 to Vglut1-ChR2 mice, Nav1.8-ChR2 displayed many more stereotypical nocifensive  
403 behaviors including licking, jumping and vocalization as intensity increased (Fig. 7C-D).  
404 Some pain-related behaviors, such as audible vocalization (Williams et al., 2008) , which  
405 were never observed in Vglut1-ChR2 mice, appeared prominently at 10  $mw/mm^2$  in  
406 Nav1.8-ChR2 mice. However, even for Nav1.8-ChR2 mice, the most numerous type of  
407 response was reflexive (Fig. 7E). Taken together, these results indicate that the behavioral  
408 responses elicited by photostimulation of cutaneous Vglut1-ChR2 neurons are likely non-  
409 nociceptive given their marked divergence from the behaviors elicited by the same stimuli  
410 in Nav1.8-ChR2 mice.

411

#### 412 **Local anesthetic and A-fiber selective blockade abolishes light-evoked** 413 **paw withdrawal**

414 To confirm that light-evoked withdrawal behaviors in Vglut1-ChR2 mice required neuronal  
415 firing, we injected the sodium channel-blocking local anesthetic ropivacaine (0.5%)  
416 subcutaneously in one hindpaw and then photostimulated both the ipsilateral and  
417 contralateral paws 30 mins post-injection at 10  $mw/mm^2$  and 10 Hz. Ipsilateral  
418 photostimulation resulted in only 10% of mice responding (1/9) but 100% responding on  
419 the contralateral side (9/9), thus confirming that light-evoked withdrawal in Vglut1-ChR2  
420 requires neuronal action potential firing (Fig. 8A). To determine more precisely whether  
421 light-evoked withdrawal behaviors in Vglut1-ChR2 were due to neuronal activity of A-  
422 fibers, we employed a combination of the Toll-like Receptor 5 (TLR5) ligand Flagellin and  
423 the membrane-impermeable sodium channel blocker QX-314, as we recently demonstrated  
424 that this mixture produces selective and reversible A-fiber blockade (Xu et al., 2015) .  
425 Because the majority (~60%) of Vglut1-ChR2 neurons express *Tlr5* (Fig. 2B,E), we  
426 predicted that this pharmacological blockade would attenuate light-evoked behaviors upon  
427 plantar photostimulation. Indeed, response frequency and number of events per trial were  
428 dramatically reduced in the ipsilateral paw 30 minutes after intraplantar injection of  
429 Flagellin/QX-314 (1  $\mu g/60mM$ ) but not vehicle (PBS) control (Fig. 8B-C). Contralateral  
430 photostimulation did not differ between the treatment groups, corroborating the specificity  
431 and of A-fiber blockade.

432

433

434 **Activation of cutaneous Vglut1-ChR2 neurons is not aversive**

435 To assess whether activation of Vglut1-ChR2-positive neurons is aversive, we adapted a  
436 two-chamber, real-time place escape/avoidance (RT-PEA) assay that was recently used to  
437 test aversion caused by optogenetic activation of TRPV1-ChR2-positive nociceptors in the  
438 trigeminal system (Rodriguez et al., 2017) (Fig. 9A). We performed this RT-PEA assay on  
439 Vglut1-ChR2 mice as well as Vglut1-EYFP control animals. Consistent with our other results  
440 supporting a non-nociceptive character of Vglut1-ChR2-positive neurons, blue light  
441 photostimulation of the plantar hindpaw did not produce statistically significant aversion  
442 during the stimulation period or the post-stimulation period in Vglut1-ChR2 mice and  
443 Vglut1-EYFP controls (Fig. 9B,E-F). In contrast, Nav1.8-ChR2 mice showed strong aversion  
444 during the stimulation period that persisted into the post-stimulation period as well,  
445 demonstrating that this RT-PEA assay can report on the aversiveness of an experience if  
446 the stimulus is adequate (Fig. 9B,E-F).

447 Because the Nav1.8-ChR2-positive population makes up a large proportion of all DRG  
448 neurons, it is possible that the observed differences in aversion behavior between Vglut1-  
449 ChR2 and Nav1.8-ChR2 mice were a consequence of the number of neurons activated  
450 rather than the distinct characteristics of the two populations. To address this possibility,  
451 we generated an additional mouse line in which ChR2 is conditionally expressed in  
452 Neuropeptide Receptor Y Receptor 2 (*Npy2r*)-positive A-mechanocceptors. *Npy2r*-ChR2-  
453 positive neurons make up a much smaller proportion of all DRG neurons than Nav1.8-ChR2  
454 neurons and thus are more comparable to the Vglut1-ChR2-positive population with  
455 respect to number of neurons that would receive photostimulation at the hindpaw (Arcourt  
456 et al., 2017). In the RT-PEA assay, *Npy2r*-ChR2 mice showed strong aversion during the  
457 stimulation period and post-stimulation period, comparable to that seen in Nav1.8-ChR2  
458 mice (Fig. 9C,E-F). Collectively, these findings indicate that optogenetic activation of Vglut1-  
459 ChR2-positive LTMRs does not produce aversion while activation of both large and small  
460 populations of nociceptors does produce strong aversion. Furthermore, these results  
461 suggest that it is type rather than number of sensory neurons activated that determines the  
462 aversiveness of a stimulus.

463

464 **Optogenetic stimulation of Vglut1-ChR2 mice in the setting of nerve**  
465 **injury-induced neuropathy**

466 Having established that cutaneous Vglut1-ChR2-positive neurons are  $A\beta$ -LTMRs and that  
467 their activation by light neither produces pain-like behaviors nor aversion in naive mice,  
468 we next sought to address the principal question of this study: Does activation of  $A\beta$ -  
469 LTMRs alone elicit nociceptive behaviors under pathological conditions? To that end, we  
470 employed the Spared Nerve Injury model (SNI) on Vglut1-ChR2 mice to induce mechanical  
471 hypersensitivity in the sural territory of the hindpaw. To minimize inter-subject variation,  
472 we used the contralateral paw as a within-subject comparison for the injured hindpaw. To

473 assess mechanical hypersensitivity from a natural mechanical stimulus, we used von Frey  
474 monofilaments to determine the 50% paw-withdrawal threshold (PWT). One week after  
475 nerve injury, on post-operative day 7 (POD7), the mice showed a marked reduction in PWT  
476 in the ipsilateral paw compared to baseline, but not the contralateral paw, consistent with  
477 previous studies using the SNI model in mice (Bourquin et al., 2006) (Fig. 10A). On POD7  
478 we tested light-evoked behaviors across a range of intensities at constant frequency (10  
479 Hz). We did not observe statistically significant differences between the ipsilateral and  
480 contralateral paws with regard to the number of any kind of behavior (Fig. 10B-D). Notably,  
481 there was no increase in affective-motivational behaviors (e.g. licking, vocalizing, guarding)  
482 in the ipsilateral paw compared to baseline or between paws.

483 To test relative aversiveness of photostimulation of the injured hindpaw, we subjected the  
484 SNI cohort to a modified version of the RT-PEA assay on POD8. In this modified RT-PEA, we  
485 applied blue light ( $10\text{ mw/mm}^2$ , 10Hz) to the sural territory of the ipsilateral hindpaw  
486 when the mouse was in its preferred chamber and to its contralateral paw when in the non-  
487 preferred chamber, analogously to the traditional PEA assay that uses von Frey filaments to  
488 assess unilateral insults (Pratt et al., 2013) . In this manner, we did not observe any  
489 changes in chamber preference during the stimulation period or the post-stimulation  
490 period, indicating that activation of Vglut1-ChR2-positive neurons in an injured hindpaw  
491 does not produce any relative aversion compared to stimulation of an uninjured hindpaw  
492 (Fig. 10E-F).

493

494

495

496

497

498

499

## 500 Discussion

501 In this study, we described a novel Vglut1-ChR2 transgenic mouse line and demonstrated  
502 its utility as a tool to activate cutaneous A $\beta$ -LTMRs via transdermal optogenetic  
503 stimulation. We exploited the Vglut1-ChR2 line to test whether specific activation of  
504 cutaneous A $\beta$ -LTMRs is sufficient to produce pain-like behaviors in the setting of  
505 neuropathy, a key outstanding question in pain research. Our findings would suggest that  
506 activation of A $\beta$ -LTMRs alone does not underlie the allodynia-like mechanical  
507 hypersensitivity observed in neuropathic pain models in mice. If true, this conclusion  
508 would warrant a reconsideration of the consensus view that A $\beta$ -LTMRs are the substrate  
509 for mechanical allodynia. While intriguing, our findings must be interpreted cautiously and  
510 in light of multiple caveats. Several lines of evidence suggest that A $\beta$ -LTMRs do contribute  
511 to mechanical allodynia in neuropathic contexts (Xu et al., 2015) . So how can we reconcile  
512 our findings with the existing body of evidence?

## 513 Type and Number of LTMR

514 First, not all A $\beta$ -LTMRs are accessed in the Vglut1-ChR2 mouse; ~50% of large-sized DRG  
515 neurons are not labeled by ChR2-EYFP and thus are not activated by photostimulation.  
516 Similarly, the incomplete overlap of ChR2-EYFP with *Vglut1* and *Tlr5* mRNA further  
517 corroborates that there are A $\beta$ -LTMRs that are not accessed. Thus, our findings can only be  
518 applied to Vglut1-ChR2-positive sensory neurons and not the entire population of A $\beta$ -  
519 LTMRs. The remaining A $\beta$ -LTMRs that do not express ChR2-EYFP in the Vglut1-ChR2  
520 mouse may be necessary to effect pain-like behaviors in the setting of injury. Alternatively,  
521 it may be that activation of only a single subtype of A $\beta$ -LTMR, either RA- or SA-A $\beta$ -LTMR, is  
522 needed to produce nociceptive behavior, and simultaneous co-activation of these two  
523 classes may actually interfere with one another; one class may be pro-nociceptive but the  
524 other could be anti-nociceptive, canceling one another and leading no net nociception.

## 525 Behavioral Assays to Assess Pain-like Behaviors

526 We measured reflexive paw withdrawal behaviors as well as real-time place aversion,  
527 approaches that have been used in the majority of similar optogenetic studies of primary  
528 sensory neurons (Draxler et al., 2014; Iyer et al., 2014; 2016; Beaudry et al., 2017) . With  
529 regard to withdrawal behaviors, our expectation was that, in the setting of nerve injury,  
530 either the number or character of the paw withdrawal behaviors would be altered.  
531 Similarly, since natural innocuous tactile stimuli can produce real-time aversion in the  
532 context of a sensitizing insult (Pratt et al., 2013), we also supposed that activating Vglut1-  
533 ChR2-positive neurons would produce aversion. We did not observe these expected  
534 outcomes. One explanation is that the behavioral assays that we used in this study may not  
535 have captured the true perceptual state of the animal, resulting in false-negative findings.  
536 That is, activation of Vglut1-ChR2-positive neurons may truly have been causing a painful  
537 perception during stimulation, but the features we measured were not able to report on  
538 that perceptual state. Indeed, a recent report by Abdus-Saboer *et al.* used high speed (1000  
539 frames per second) video to analyze paw withdrawal responses to natural and optogenetic  
540 stimuli and found that the features that most strongly distinguished withdrawal to noxious



541 stimuli from innocuous stimuli were paw height, paw velocity, and a composite “pain  
542 score”, features that we were unable to measure in this study (Abdus-Saboor et al., 2018).  
543 In a similar vein, it may be the case that the relevant behavioral features or ‘syllables’ that  
544 reflect the true underlying pain state are unrelated to anything we measured, and instead  
545 should be discerned using unsupervised analysis, similar to the approach by Wiltchko *et al.*  
546 (Wiltchko et al., 2015). Future studies applying these advanced behavioral methods to  
547 Vglut1-ChR2 mice may lead to different conclusions than the ones we reached in this study.

#### 548 **Comparison to Other Optogenetic Studies of LTMRs in Pain**

549 While preparing this manuscript, two studies were published that also examined the  
550 contribution of  $A\beta$ -LTMRs in pathological pain using optogenetics (Dhandapani et al.,  
551 2018). Dhandapani *et al.* used a mouse expressing tamoxifen-inducible Cre recombinase in  
552 frame with TrkB (TrkB-CreERT2) to access a mixed population of PSNs comprised of  $A\beta$   
553 RA-LTMRs and  $A\delta$ -LTMRs (D-hairs). They showed that in the SNI model, TrkB-ChR2 mice  
554 showed increased response frequency at POD7 compared to baseline along with the  
555 appearance of nocifensive responses to light (e.g. licking, prolonged lifting). Using toxin-  
556 mediated ablation, they also showed the necessity of *TrkB*-positive neurons for allodynia-  
557 like behaviors in the SNI model. We saw neither increased numbers of responses nor the  
558 appearance of nocifensive (i.e. affective-motivational) behaviors at POD7 in the SNI model  
559 using similar stimulation conditions. One likely explanation for the different behavioral  
560 findings in our study is that Vglut1-ChR2 does not access the neuronal population that  
561 caused the pain-like behaviors in the Dhandapani study. While both TrkB-ChR2 and Vglut1-  
562 ChR2 label Ret-positive  $A\beta$  RA-LTMRs, the Vglut1-ChR2 population does not overlap with  
563 the large majority of highly expressing *TrkB*-positive neurons (*TrkB<sup>High</sup>*), which are most  
564 likely  $A\delta$ -LTMRs (Usoskin et al., 2014). Light stimulation of the sural territory inevitably  
565 shines on some hairy skin since the boundary between hairy and glabrous skin lies in this  
566 area. Thus, photostimulation of TrkB-positive  $A\delta$ -LTMRs may have occurred, giving rise to  
567 pain-like responses. Thus, it is reasonable to suggest that  $A\delta$ -LTMRs mediated the positive  
568 pain-like behaviors in the Dhandapani study in the SNI model. If true, our study  
569 complements the findings from the Dhandapani study and suggests further refinement as  
570 to which population of LTMR is sufficient to elicit pain-like behaviors in nerve injury-  
571 induced neuropathy.

572 Similarly, a study from Tashima *et al.* used an optogenetic approach to test the contribution  
573 of  $A\beta$ -LTMRs to pain-like behaviors in nerve injury-induced neuropathy (Tashima et al.,  
574 2018). They used a transgenic rat that expresses ChR2 broadly in non-nociceptive sensory  
575 neurons, some of which are  $A\beta$ -LTMRs, under the control of the *Thy1* promoter(W-  
576 TChr2V4) (Ji et al., 2012). They showed that in rats that received unilateral peripheral  
577 nerve injury (Spinal Nerve Transection model), photostimulation elicited pain-like  
578 behaviors on the ipsilateral paw but not on the contralateral paw. They also showed that  
579 injured rats exhibited light-evoked place aversion but naive rats did not. How to explain the  
580 discrepancy? First, light-evoked withdrawal in the uninjured paw “produced no reaction or  
581 only mild movement without any lifting or flinching behaviors” (Tashima et al., 2018),  
582 which presumably would also be true in naive animals. Accordingly, because the basal  
583 light-evoked behavior is a non-response, the changes that occurred on the injured paw

584 were readily apparent and distinct. In contrast, in our study, even at the lowest intensity (1  
585  $mw/mm^2$ ), the animals showed responses, and at the higher intensities (5-10  $mw/mm^2$ )  
586 they almost always responded, making it more challenging to see differences due to  
587 perturbations. Another key difference is the stimulation paradigm used by Tashima *et al.*  
588 They used relatively long pulse widths (500 ms) at very low frequency (0.1 Hz), whereas  
589 we used 5-10ms pulse widths and 1-10Hz pulsed stimulation, in line with most other  
590 studies looking at peripheral optogenetic stimulation. We selected this stimulation protocol  
591 because it has been shown that continuous light causes ChR2 to desensitize(Nagel *et al.*,  
592 2003) and that long pulse-widths (>50 ms) can silence many kinds of neurons by inducing  
593 depolarization block (Herman *et al.*, 2014). Indeed, we confirmed this using whole-cell  
594 patch-clamp in DRGs from Vglut1-ChR2 mice *in vitro* using constant light, where only a  
595 single action potential was elicited at the onset of illumination followed by a constant,  
596 subthreshold depolarization. The nature of the electrophysiological effects *in vivo* caused  
597 by 500 ms pulses in the study by Tashima *et al.* are uncertain, but likely differed from ours.  
598 This difference may account for the divergent findings. Also, as mentioned for the  
599 Dhandapani study, the populations of neurons accessed in the W-TChR2V4 rat may differ  
600 substantially from our Vglut1-ChR2 mouse. Furthermore, species differences (i.e rat  
601 vs. mouse) or differences in nerve injury model (SNI vs. SNT) could account for our  
602 different findings. Regardless, this important study by Tashima *et al.* definitively  
603 demonstrated that a non-nociceptive population of LTMR can produce pain-like behaviors  
604 in specific contexts. Understanding and defining those contexts will be an important area of  
605 future investigation.

606 Despite these limitations, our study makes several interesting observations. The Vglut1-  
607 ChR2 mouse, as well as the Vglut1-Cre driver used to generate it, will be broadly useful for  
608 the study of pain and touch. While there are numerous mouse lines to access various kinds  
609 of nociceptors(Cavanaugh *et al.*, 2011) , relatively few lines target  $A\beta$ -LTMRs. The Vglut1-  
610 Cre line expands the growing arsenal of Cre lines to target primary sensory neurons and  
611 complements the existing lines that access more restricted subpopulations of  $A\beta$ -LTMRs  
612 such as RetCreERT2(Luo *et al.*, 2009) , TrkB-CreERT2(Dhandapani *et al.*, 2018) and TrkC-  
613 CreERT2(Rutlin *et al.*, 2014) . The Vglut1-ChR2 mouse in particular could be used to study  
614 the contribution of LTMRs in other pain and itch conditions not tested here  
615 (e.g. inflammatory, chemotherapy). And the Vglut1-Cre line can be used to express other  
616 opsins, fluorophores, or for the conditional manipulation of natively expressed genes. The  
617 intensive behavioral characterization we performed sheds light on the different behavioral  
618 signatures of non-nociceptive and nociceptive neuronal activation, and highlights the  
619 importance of measuring features beyond just paw lifting, which is a seemingly universal  
620 response across optogenetic mouse lines(Draxler *et al.*, 2014; Iyer *et al.*, 2014; 2016;  
621 Beaudry *et al.*, 2017). The RT-PEA assay that we adapted expands the arsenal of ways that  
622 one can use transdermal optogenetics to study pain and will be useful in the study of other  
623 optogenetic lines. And, at least in the case of the SNI model, our findings refine our  
624 understanding of the contribution of  $A\beta$ -LTMRs to neuropathic pain.



625 **Acknowledgements**

626 We thank Yawar Qadri for critical reading of the manuscript. This study is supported in  
627 part by R01DE17794 and R01NS87988 (R-R.J) and Congressionally Directed Medical  
628 Research Programs and the Department of Defense awards W81XWH-12-2-0129 and  
629 W81XWH-15-2-0046(TV).

630 **References**

631

632 Agarwal N, Offermanns S, Kuner R (2004) Conditional gene deletion in primary nociceptive  
633 neurons of trigeminal ganglia and dorsal root ganglia. *genesis* 38:122–129.

634 Alvarez FJ, Villalba RM, Zerda R, Schneider SP (2004) Vesicular glutamate transporters in  
635 the spinal cord, with special reference to sensory primary afferent synapses. *J Comp*  
636 *Neurol* 472:257–280.

637 Arcourt A, Gorham L, Dhandapani R, Prato V, Taberner FJ, Wende H, Gangadharan V,  
638 Birchmeier C, Heppenstall PA, Lechner SG (2017) Touch Receptor-Derived Sensory  
639 Information Alleviates Acute Pain Signaling and Fine-Tunes Nociceptive Reflex  
640 Coordination. *Neuron* 93:179–193.

641 Bai L, Lehnert BP, Liu J, Neubarth NL, Dickendeshler TL, Nwe PH, Cassidy C, Woodbury CJ,  
642 Ginty DD (2015) Genetic Identification of an Expansive Mechanoreceptor Sensitive to  
643 Skin Stroking. *Cell* 163:1783–1795.

644 Bankhead P, Loughrey MB, Fernández JA, Dombrowski Y, McArt DG, Dunne PD, McQuaid S,  
645 Gray RT, Murray LJ, Coleman HG, James JA, Salto-Tellez M, Hamilton PW (2017)  
646 QuPath: Open source software for digital pathology image analysis. *Sci Rep* 7:16878.

647 Basbaum AI, Bautista DM, Scherrer G, Julius D (2009) Cellular and molecular mechanisms  
648 of pain. *Cell* 139:267–284.

649 Beaudry H, Daou I, Ase AR, Ribeiro-da-Silva A, Séguéla P (2017) Distinct behavioral  
650 responses evoked by selective optogenetic stimulation of the major TRPV1+ and MrgD+  
651 subsets of C-fibers. *PAIN* 158:2329–2339.

652 Berta T, Perrin FE, Pertin M, Tonello R, Liu Y-C, Chamessian A, Kato AC, Ji R-R, Decosterd I  
653 (2017) Gene Expression Profiling of Cutaneous Injured and Non-Injured Nociceptors in  
654 SNI Animal Model of Neuropathic Pain. *Sci Rep* 7:9367.

655 Bonin RP, Bories C, De Koninck Y (2014) A simplified up-down method (SUDO) for  
656 measuring mechanical nociception in rodents using von Frey filaments. *Mol Pain* 10:26.

- 657 Bourane S, Garces A, Ventéo S, Pattyn A, Hubert T, Fichard A, Puech S, Boukhaddaoui H,  
658 Baudet C, Takahashi S, Valmier J, Carroll P (2009) Low-Threshold Mechanoreceptor  
659 Subtypes Selectively Express MafA and Are Specified by Ret Signaling. *Neuron* 64:857–  
660 870.
- 661 Bourquin A-F, Süveges M, Pertin M, Gilliard N, Sardy S, Davison AC, Spahn DR, Decosterd I  
662 (2006) Assessment and analysis of mechanical allodynia-like behavior induced by  
663 spared nerve injury (SNI) in the mouse. *PAIN* 122:14.e1–.e14.
- 664 Brumovsky P, Watanabe M, Hökfelt T (2007) Expression of the vesicular glutamate  
665 transporters-1 and -2 in adult mouse dorsal root ganglia and spinal cord and their  
666 regulation by nerve injury. *NSC* 147:469–490.
- 667 Cavanaugh DJ, Chesler AT, Jackson AC, Sigal YM, Yamanaka H, Grant R, O'Donnell D, Nicoll  
668 RA, Shah NM, Julius D, Basbaum AI (2011) Trpv1 Reporter Mice Reveal Highly  
669 Restricted Brain Distribution and Functional Expression in Arteriolar Smooth Muscle  
670 Cells. *Journal of Neuroscience* 31:5067–5077.
- 671 Chang RB, Strohlic DE, Williams EK, Umans BD, Liberles SD (2015) Vagal Sensory Neuron  
672 Subtypes that Differentially Control Breathing. *Cell* 161:622–633.
- 673 Corder G, Tawfik VL, Wang D, Sypek EI, Low SA, Dickinson JR, Sotoudeh C, Clark JD, Barres  
674 BA, Bohlen CJ, Scherrer G (2017) Loss of  $\mu$  opioid receptor signaling in nociceptors, but  
675 not microglia, abrogates morphine tolerance without disrupting analgesia. *Nat Med*  
676 23:164–173.
- 677 da Silva Serra I, Husson Z, Bartlett JD, Smith ESJ (2016) Characterization of cutaneous and  
678 articular sensory neurons. *Mol Pain* 12:174480691663638.
- 679 Daou I, Tuttle AH, Longo G, Wieskopf JS, Bonin RP, Ase AR, Wood JN, De Koninck Y, Ribeiro-  
680 da-Silva A, Mogil JS, Seguela P (2013) Remote Optogenetic Activation and Sensitization  
681 of Pain Pathways in Freely Moving Mice. *Journal of Neuroscience* 33:18631–18640.
- 682 Dhandapani R, Arokiaraj CM, Taberner FJ, Pacifico P, Raja S, Nocchi L, Portulano C,  
683 Franciosa F, Maffei M, Hussain AF, Reis FC, Reymond L, Perlas E, Garcovich S, Barth S,  
684 Johnsson K, Lechner SG, Heppenstall PA (2018) Control of mechanical pain  
685 hypersensitivity in mice through ligand-targeted photoablation of TrkB-positive  
686 sensory neurons. *Nat Comms* 9:1640.
- 687 Draxler P, Honsek SD, Forsthuber L, Hadschieff V, Sandkuhler J (2014) VGlut3 primary  
688 afferents play distinct roles in mechanical and cold hypersensitivity depending on pain  
689 etiology. *Journal of Neuroscience* 34:12015–12028.
- 690 Ewan St John Smith GRL (2009) Nociceptors: a phylogenetic view. *Journal of Comparative*  
691 *Physiology A, Neuroethology, Sensory, Neural, and Behavioral Physiology* 195:1089–  
692 1106.

- 693 Friard O, Gamba M (2016) BORIS: a free, versatile open-source event-logging software for  
694 video/audio coding and live observations Fitzjohn R, ed. *Methods in Ecology and*  
695 *Evolution* 7:1325–1330.
- 696 Harris JA, Hirokawa KE, Sorensen SA, Gu H, Mills M, Ng LL, Bohn P, Mortrud M, Ouellette B,  
697 Kidney J, Smith KA, Dang C, Sunkin S, Bernard A, Oh SW, Madisen L, Zeng H (2014)  
698 Anatomical characterization of Cre driver mice for neural circuit mapping and  
699 manipulation. *Front Neural Circuits* 8.
- 700 Herman AM, Huang L, Murphey DK, Garcia I, Arenkiel BR (2014) Cell type-specific and  
701 time-dependent light exposure contribute to silencing in neurons expressing  
702 Channelrhodopsin-2. *eLife* 3:e01481.
- 703 Iyer SM, Montgomery KL, Towne C, Lee SY, Ramakrishnan C, Deisseroth K, Delp SL (2014)  
704 Virally mediated optogenetic excitation and inhibition of pain in freely moving  
705 nontransgenic mice. *Nat Biotechnol* 32:274–278.
- 706 Iyer SM, Vesuna S, Ramakrishnan C, Huynh K, Young S, Berndt A, Lee SY, Gorini CJ,  
707 Deisseroth K, Delp SL (2016) Optogenetic and chemogenetic strategies for sustained  
708 inhibition of pain. *Sci Rep* 6:30570.
- 709 Ji Z-G, Ito S, Honjoh T, Ohta H, Ishizuka T, Fukazawa Y, Yawo H (2012) Light-evoked  
710 Somatosensory Perception of Transgenic Rats That Express Channelrhodopsin-2 in  
711 Dorsal Root Ganglion Cells Baccei ML, ed. *PLoS ONE* 7:e32699.
- 712 Latremoliere A, Woolf CJ (2009) Central Sensitization: A Generator of Pain Hypersensitivity  
713 by Central Neural Plasticity. *The Journal of Pain* 10:895–926.
- 714 Lolignier S, Eijkelkamp N, Wood JN (2015) Mechanical allodynia. *Pflugers Arch - Eur J*  
715 *Physiol* 467:133–139.
- 716 Luo W, Enomoto H, Rice FL, Milbrandt J, Ginty DD (2009) Molecular identification of rapidly  
717 adapting mechanoreceptors and their developmental dependence on ret signaling.  
718 *Neuron* 64:841–856.
- 719 Madisen L et al. (2012) A toolbox of Cre-dependent optogenetic transgenic mice for light-  
720 induced activation and silencing. *Nat Neurosci* 15:793–802.
- 721 Madisen L, Zwingman TA, Sunkin SM, Oh SW, Zariwala HA, Gu H, Ng LL, Palmiter RD,  
722 Hawrylycz MJ, Jones AR, Lein ES, Zeng H (2010) A robust and high-throughput Cre  
723 reporting and characterization system for the whole mouse brain. *Nat Neurosci*  
724 13:133–140.
- 725 Nagel G, Szellas T, Huhn W, Kateriya S, Adeishvili N, Berthold P, Ollig D, Hegemann P,  
726 Bamberg E (2003) Channelrhodopsin-2, a directly light-gated cation-selective  
727 membrane channel. *Proc Natl Acad Sci USA* 100:13940–13945.

- 728 Pratt D, Fuchs PN, Sluka KA (2013) Assessment of avoidance behaviors in mouse models of  
729 muscle pain. *Neuroscience* 248:54–60.
- 730 Rodriguez E, Sakurai K, Xu J, Chen Y, Toda K, Zhao S, Han B-X, Ryu D, Yin H, Liedtke W,  
731 Wang F (2017) A craniofacial-specific monosynaptic circuit enables heightened  
732 affective pain. *Nat Neurosci* 20:1734–1743.
- 733 Rogoz K, Lagerström MC, Dufour S, Kullander K (2012) VGLUT2-dependent glutamatergic  
734 transmission in primary afferents is required for intact nociception in both acute and  
735 persistent pain modalities. - PubMed - NCBI. *PAIN* 153:1525–1536.
- 736 Rutlin M, Ho C-Y, Abraira VE, Cassidy C, Bai L, Woodbury CJ, Ginty DD (2014) The Cellular  
737 and Molecular Basis of Direction Selectivity of A $\delta$ -LTMRs. *Cell* 159:1640–1651.
- 738 Srinivas S, Watanabe T, Lin CS, William CM, Tanabe Y, Jessell TM, Costantini F (2001) Cre  
739 reporter strains produced by targeted insertion of EYFP and ECFP into the ROSA26  
740 locus. *BMC Dev Biol* 1:4.
- 741 Tashima R, Koga K, Sekine M, Kanehisa K, Kohro Y, Tominaga K, Matsushita K, Tozaki-  
742 Saitoh H, Fukazawa Y, Inoue K, Yawo H, Furue H, Tsuda M (2018) Optogenetic  
743 Activation of Non-Nociceptive A $\beta$  Fibers Induces Neuropathic Pain-Like Sensory and  
744 Emotional Behaviors after Nerve Injury in Rats. *eneuro* 5:ENEURO.0450–17.2018.
- 745 Todd AJ, Hughes DI, Polgár E, Nagy GG, Mackie M, Ottersen OP, Maxwell DJ (2003) The  
746 expression of vesicular glutamate transporters VGLUT1 and VGLUT2 in  
747 neurochemically defined axonal populations in the rat spinal cord with emphasis on the  
748 dorsal horn. *Eur J Neurosci* 17:13–27.
- 749 Torebjörk HE, Lundberg LE, LaMotte RH (1992) Central changes in processing of  
750 mechanoreceptive input in capsaicin-induced secondary hyperalgesia in humans. *The*  
751 *Journal of Physiology* 448:765–780.
- 752 Usoskin D, Furlan A, Islam S, Abdo H, Lönnerberg P, Lou D, Hjerling-Leffler J, Haeggström J,  
753 Kharchenko O, Kharchenko PV, Linnarsson S, Ernfors P (2014) Unbiased classification  
754 of sensory neuron types by large-scale single-cell RNA sequencing. *Nat Neurosci*.
- 755 Williams WO, Riskin DK, Mott AKM (2008) Ultrasonic sound as an indicator of acute pain in  
756 laboratory mice. *Journal of the American Association for Laboratory Animal Science* :  
757 *JAALAS* 47:8–10.
- 758 Wiltschko AB, Johnson MJ, Iurilli G, Peterson RE, Katon JM, Pashkovski SL, Abraira VE,  
759 Adams RP, Datta SR (2015) Mapping Sub-Second Structure in Mouse Behavior. *Neuron*  
760 88:1121–1135.
- 761 Xu Z-Z, Kim YH, Bang S, Zhang Y, Berta T, Wang F, Oh SB, Ji R-R (2015) Inhibition of  
762 mechanical allodynia in neuropathic pain by TLR5-mediated A-fiber blockade. *Nat Med*  
763 21:1326–1331.

764 Zimmerman A, Bai L, Ginty DD (2014) The gentle touch receptors of mammalian skin.  
765 Science 346:950–954.

766

## 767 Figure Captions

768

769 **Figure 1 Cellular distribution of Chr2-EYFP in dorsal root ganglia:** (A), Chr2-EYFP co-  
770 expression with selected markers in DRG. Scale bar: 50  $\mu$ m. (B, C), Quantification of co-  
771 expression of Chr2-EYFP with selected markers (Mean  $\pm$  SEM, n=4 animals, 3-4  
772 sections/animal). (D), Size Distribution of all (Total) and Chr2-EYFP-positive DRG neurons,  
773 expressed as probability density. (E), Proportion of Chr2-EYFP-positive neurons in each size  
774 class of DRG neuron. Small: < 300 $\mu$ m, Medium: 300-600  $\mu$ m, Large: >600  $\mu$ m. Values inside  
775 bars represent the number of Chr2-EYFP-positive (green) and Chr2-EYFP-negative (grey)  
776 neurons in each size class (n=6 animals, 2-3 sections/animal)

777

778 **Figure 2 Co-expression with A $\beta$ -LTMR markers** Co-expression of Chr2-EYFP with Nefh and  
779 Ret (A) and Tlr5 (B), Scale Bar: 50  $\mu$ m. Arrows indicate cells that co-express all markers. (C),  
780 Venn Diagram of Chr2-EYFP, Nefh and Ret. (D-E), Quantification of co-expression for Chr2-  
781 EYFP, Nefh, and Ret represented as percent (%) of population (Mean  $\pm$  SEM, n=6 animals, 2-3  
782 sections/animal)

783

784 **Figure 3 Expression of TrkB in Vglut1-Chr2 DRG (Left)**, Co-expression of Chr2-EYFP  
785 transcript by ISH. Arrow indicates a Chr2-EYFP-positive neuron co-expressing low levels of  
786 TrkB. Asterisk indicates highly-expressing TrkB-positive neurons that lack Chr2-EYFP  
787 expression, which are likely A $\delta$ -LTMRs. Note the expression of TrkB around the  
788 circumference of Chr2-EYFP-positive neurons, likely in Satellite Glia Cells. Scale: 50 $\mu$ m.  
789 (Right), Zoom of inset.

790

791 **Figure 4 Spinal and cutaneous projections of Chr2-EYFP-positive neurons in Vglut1-  
792 Chr2.** (A), Low magnification of Chr2-EYFP-positive afferents in the lumbar spinal cord  
793 (Top), Scale: 500  $\mu$ m. High magnification images of Chr2-EYFP-positive, CGRP+ and IB4+  
794 afferents in the dorsal horn (Bottom), Scale: 100  $\mu$ m. Lamina borders (white) are  
795 represented in the Merged image. (B), Cutaneous Projections of Chr2-EYFP-positive afferents in  
796 glabrous (Top, Mid), and Hairy (Bottom) skin. In the top panel, Chr2-EYFP-positive afferents  
797 make direct contacts with TROMA1-positive (red) Merkel Cells in glabrous skin. Scale: 10  
798  $\mu$ m.

799

800 **Figure 5 Patch-clamp electrophysiology of Chr2-EYFP-positive and Chr2-EYFP-negative  
801 DRG neurons** (A), Continuous exposure to 470 nm light for 1s resulted in depolarization and



802 light-evoked action potentials in ChR2-EYFP-positive DRG neurons (black) but not ChR2-  
 803 EYFP-negative neurons (red). **(B)**, Exposure to light at 10 Hz drove phase-locked action  
 804 potential firing in ChR2-EYFP-positive DRG neurons (black) but not ChR2-EYFP-negative  
 805 controls (red). **(C-D)** The success rate at 5Hz and 10Hz photostimulation of ChR2-EYFP-  
 806 positive (n=7) and ChR2-EYFP-negative (n=4) neurons. **(E)** Representative action potential  
 807 waveforms from ChR2-EYFP-positive(top) and ChR2-EYFP-negative (bottom) DRG neurons. .  
 808 **(F)**, The width of the action potential waveform at half-maximum amplitude of ChR2-EYFP-  
 809 positive and ChR2-EYFP-negative DRG neurons (Student's two-tailed t-test, \*  $p < 0.05$ ) **(G)**.  
 810 The action potential threshold of ChR2-EYFP-positive and ChR2-EYFP-negative DRG neurons  
 811 (Student's two-tailed t-test, \*\*  $p < 0.005$ ). **(H)** The number of spikes under continuous  
 812 photostimulation in ChR2-EYFP positive and ChR2-EYFP-negative neurons. Panels C-D, F-H  
 813 represented as mean  $\pm$  SEM.

814

815 **Figure 6 Light-evoked withdrawal behaviors in naive Vglut1-ChR2 Mice** **(A)**, Response  
 816 frequency (i.e. fraction of all trials with at least one response per trial) increases with the  
 817 intensity and frequency of light stimulation (n=14). **(B)**, The total number of all behavioral  
 818 responses increases with intensity and frequency of light stimulation (n=14). **(C)**, Dot plot  
 819 representation of individual scored behaviors at each intensity and frequency combination.  
 820 The size of each dot represents the percent of trials in which the behavior was observed, and  
 821 the color represents the total number of a given behavior per trial, with red indicating higher  
 822 numbers and blue indicating lower numbers. **(D-E)**, The number of affective-motivational and  
 823 reflexive responses per trial. Panels A-B, D-E represented as mean  $\pm$  SEM.

824

825 **Figure 7 Comparison of light-evoked withdrawal behaviors in Vglut1-ChR2 and Nav1.8-**  
 826 **ChR2 mice.** **(A)**, The response frequency of Vglut1-ChR2 is lower than that of Nav1.8-ChR2 at  
 827 all intensities (Genotype:  $F_{(1,59)} = 51.99$ ,  $p < 0.001$ . Intensity:  $F_{(3,59)} = 11.07$ ,  $p < 0.001$ ,  
 828 Genotype x Intensity  $F_{(3,59)} = 3.57$ ,  $p = 0.02$ ). **(B)**, The total number of responses is  
 829 substantially lower in Vglut1-ChR2 compared to Nav1.8-ChR2 (Genotype:  $F_{(1,59)} = 2034.68$ ,  $p$   
 830  $< 0.001$ , Intensity:  $F_{(3,59)} = 169.50$ ,  $p < 0.001$ , Genotype x Intensity:  $F_{(3,59)} = 282.0273$ ,  $p <$   
 831  $0.001$ ). **(C)**, The behavioral signatures of Vglut1-ChR2 and Nav1.8-ChR2 differ markedly. Dot  
 832 plot representation of individual scored behaviors at each intensity and frequency  
 833 combination. The size of each dot represents the percent of trials in which the behavior was  
 834 observed, and the color represents the total number of a given behavior per trial, with red  
 835 indicating higher numbers and blue indicating lower numbers. **(D)**, Affective-motivational  
 836 behaviors increase with intensity in Nav1.8-ChR2 but are absent in Vglut1-ChR2 (Genotype:  
 837  $F_{(1,59)} = 176.01$ ,  $p < 0.001$ , Intensity:  $F_{(3,59)} = 13.03$ ,  $p < 0.001$ , Genotype x Intensity:  
 838  $F_{(3,59)} = 31.75$ ,  $p < 0.001$ ). **(E)**, The number of reflexive responses is higher at all intensities  
 839 in Nav1.8-ChR2 (Genotype:  $F_{(1,59)} = 964.03$ ,  $p < 0.001$ , Intensity:  $F_{(3,59)} = 86.67$ ,  $p < 0.001$ ,  
 840 Genotype x Intensity:  $F_{(3,59)} = 127.67$ ,  $p < 0.001$ ). Statistical Analysis: Two-Factor Linear  
 841 Mixed Effects (LME) model, Tukey's post-hoc tests. Vglut1-ChR2 (n=14), Nav1.8-ChR2 (n=6) for  
 842 all panels. Post-hoc tests: Vglut1-ChR2 vs. Nav1.8-ChR2 at each intensity, \*\* $p < 0.01$ , \*\*\* $p <$

843 0.001. Panels A-B, D-E represented as mean±SEM. Note: The data presented here for Vglut1-  
844 Chr2 (2 Hz) are re-plotted from Figure 6.

845

846 **Figure 8 Local anesthetic and A-fiber selective blockade abolishes light-evoked paw**  
847 **withdrawal (A)**, Intraplantar (I.pl) Ropivacaine (0.5%, 20µl) blocked light-evoked paw  
848 withdrawal in 8/9 mice (n=9) in the ipsilateral (left) paw, but all mice (9/9) responded to  
849 stimulation of the uninjected, contralateral paw. **(B)** Light-evoked response frequency was  
850 strongly attenuated in the ipsilateral (Ipsi) paw of Vglut1-ChR2 mice that received A-fiber  
851 blockade with QX-314/Flagellin (60 mM/1µg, 20 µl, I. pl) but not Vehicle control (PBS,  
852 20µl, i. Pl).(Treatment:  $F_{(1,12)} = 13.58, p=0.0031$ , Paw:  $F_{(1,54)} = 8.00, p = 0.0066$ , Treatment  
853 x Paw:  $F_{(1,54)} = 20.3, p <.0001$ ). **(C)** The number of light-evoked responses was also strongly  
854 attenuated by QX-314/Flagellin (Treatment:  $F_{(1,12)} = 12.88, p=0.0037$ , Paw:  $F_{(1,54)} = 1.05,$   
855  $p = 0.31$ , Treatment x Paw:  $F_{(1,54)} = 9.97, p 0.0026$ ). For B-C, in both treatment groups, the  
856 contralateral (Contra) uninjected paw was stimulated after ipsilateral stimulation to  
857 demonstrate the localized nature of A-fiber blockade and confirm the responsiveness of each  
858 subject (n=7/group, Stimulation: 5 mW/mm<sup>2</sup>, 10 Hz). Statistical analysis: Two-factor Linear  
859 Mixed Effects (LME) model, Tukey's post-hoc test. Panels B-C represented as mean±SEM. Post-  
860 hoc test: \*\*p <0.01, \*\*\*p<0.001.

861

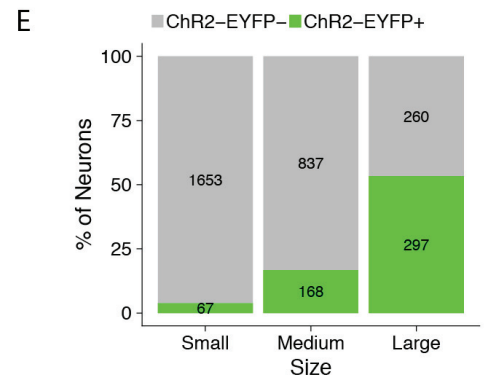
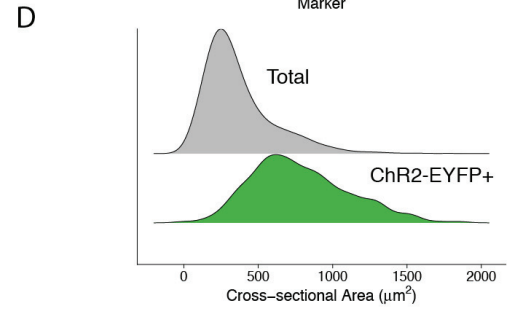
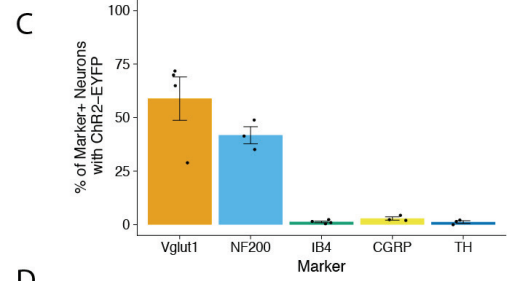
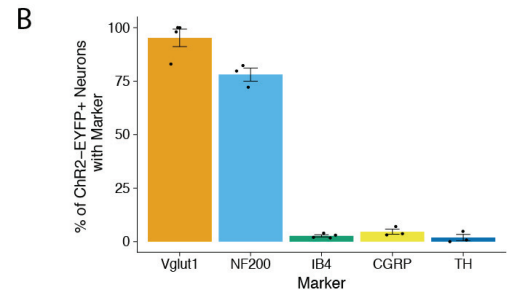
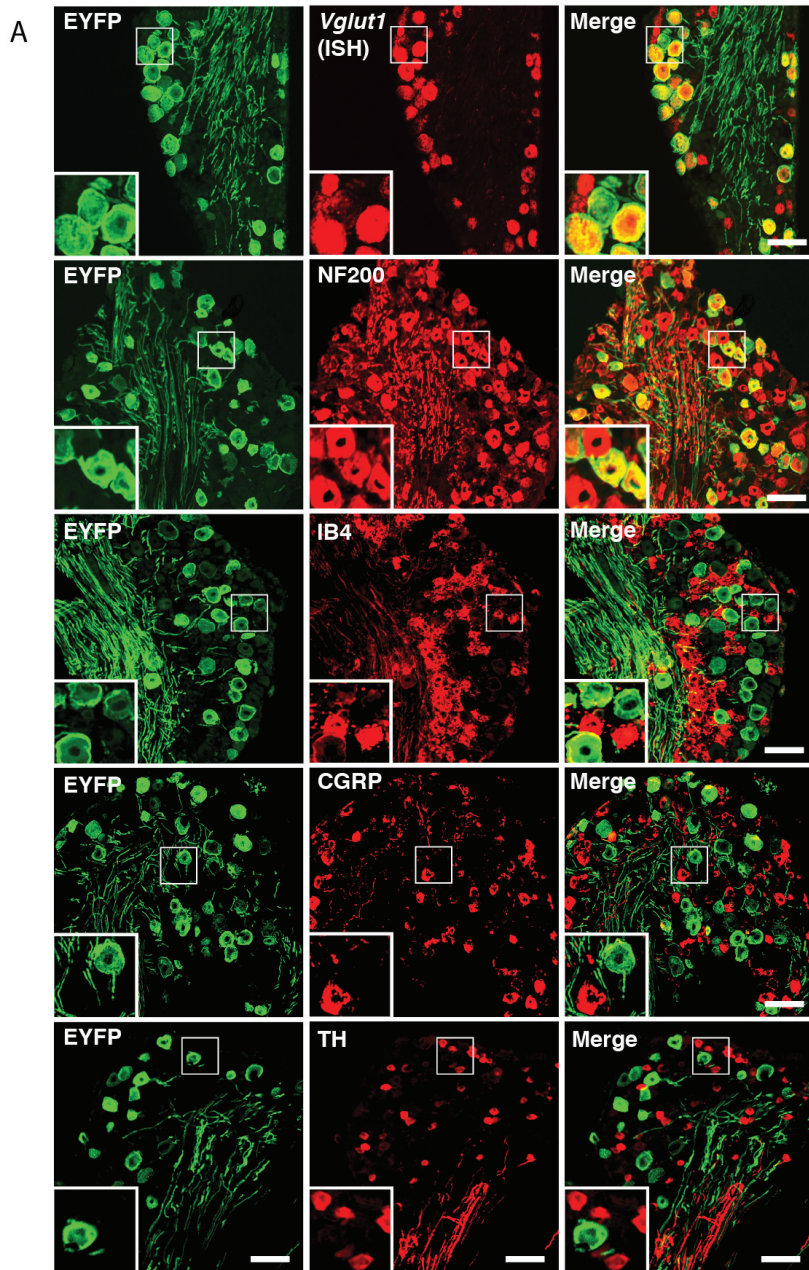
862 **Figure 9 Real-time place escape-avoidance assay (RT-PEA) in non-nociceptive and**  
863 **nociceptive Chr2-expressing mouse line (A)**, Schematic of RT-PEA assay. The assay is  
864 divided into three 10 min stages: Pre-stimulation (Pre), Stimulation (Stim), and Post-  
865 stimulation (Post). During the Pre period, mice are allowed to freely explore both sides of the  
866 chamber apparatus. During the Stim period, mice are stimulated with blue light in their  
867 preferred chamber and with yellow light in their non-preferred chamber. During the Post  
868 period, mice freely moved between chambers without stimulation. **(B-C)**, Blue light  
869 stimulation causes strong aversion in nociceptive (Nav1.8-ChR2 and Npy2r-ChR2) but not  
870 non-nociceptive mice (Vglut1-ChR2 and Vglut1-EYFP). (Vglut1-ChR2, Stage:  $F_{(2,26)} = 2.44, p$   
871  $= 0.11, n=14$ . Vglut1-EYFP, Stage:  $F_{(2,12)} = 0.17, p = 0.85, n=7$ . Nav1.8-ChR2, Stage:  
872  $F_{(2,10)} = 96.39, p <0.000, n=6$ , Npy2r-ChR2, Stage:  $F_{(2,12)} = 33.27, p < 0.0001, n=7$ ). **(D-E)**, RT-  
873 PEA assay results represented as change from baseline (Pre) preference (%).(Vglut1-ChR2,  
874 Stage:  $F_{(2,26)} = 2.40, p = 0.11$ . Vglut1-EYFP, Stage:  $F_{(2,12)} = 0.25, p = 0.78$ . Nav1.8-ChR2,  
875 Stage:  $F_{(2,10)} = 144.8, p <0.0001$ , Npy2r-ChR2, Stage:  $F_{(2,12)} = 38.39, p < 0.0001$ ). **(F)**,  
876 Representative spatial heat maps for each mouse line. Yellow indicates more time spent in the  
877 area and blue indicates less time spent in the area. NP: Non-Preferred Chamber, P: Preferred  
878 Chamber. Statistical analysis: One-Factor Linear Mixed Effects (LME) model for each line,  
879 with Tukey's post-hoc test. Post-hoc tests: \*\*, p <0.01, \*\*\*, p <0.001, NS = Not Significant  
880 (p>0.05). Panels B-E represented as mean±SEM.

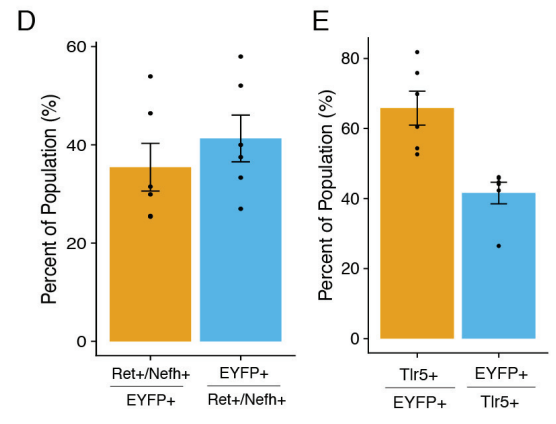
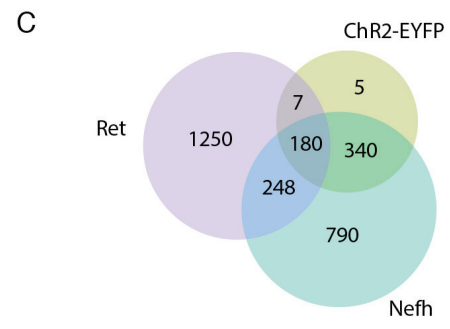
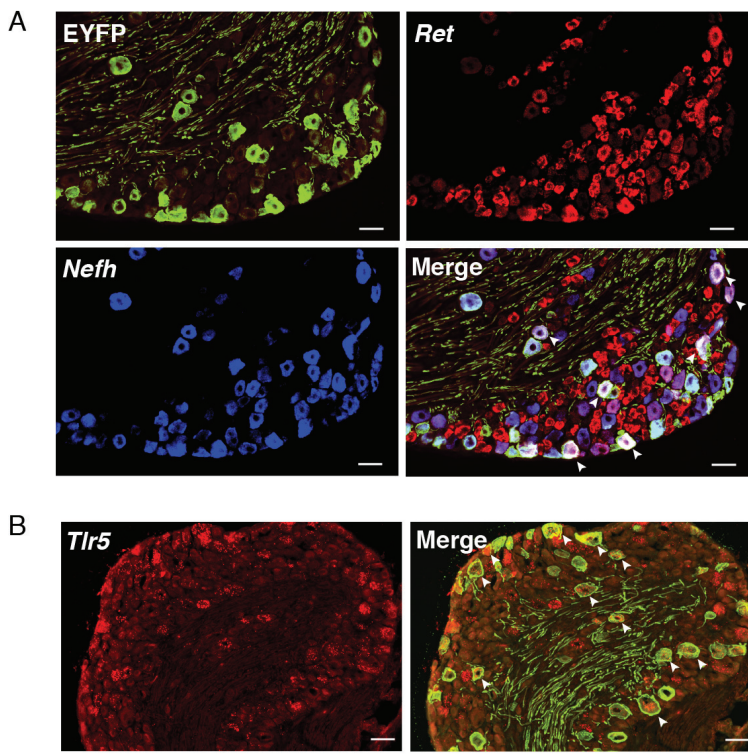
881

882 **Figure 10 Optogenetic stimulation of SNI mice does not elicit pain-like behaviors or**  
883 **aversion (A)**, Spared Nerve Injury causes decreased paw withdrawal thresholds (PWT) in the

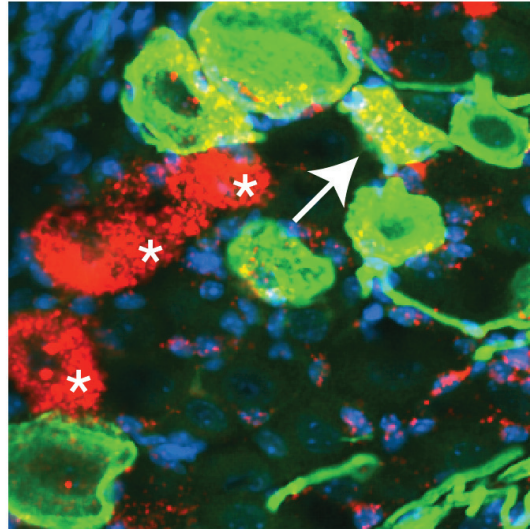
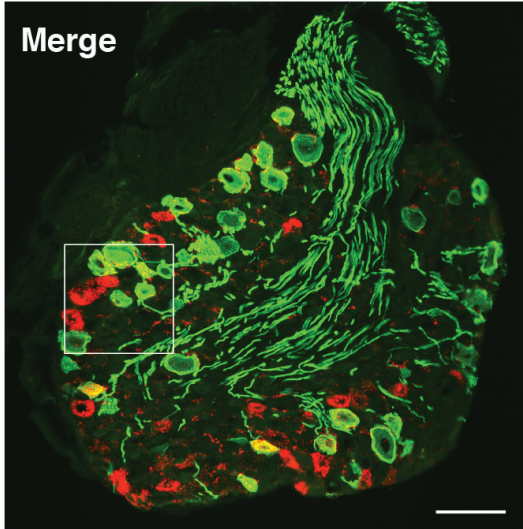
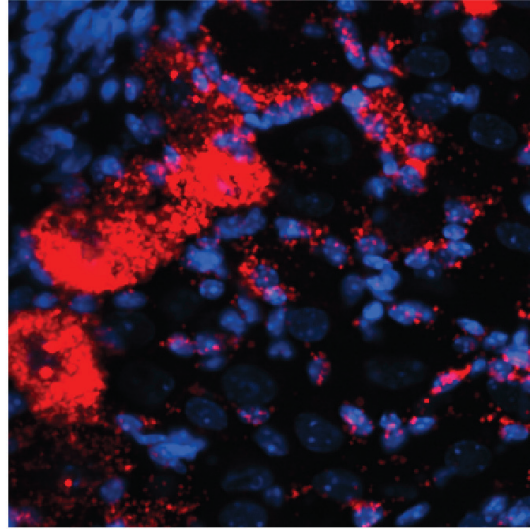
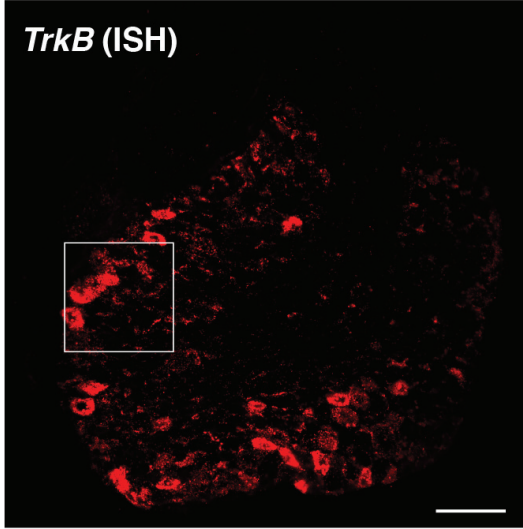
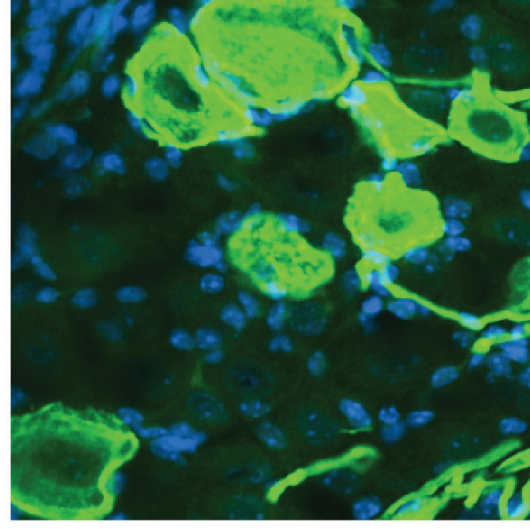
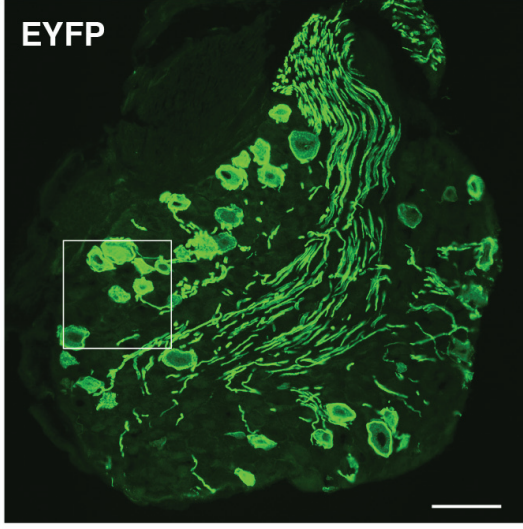


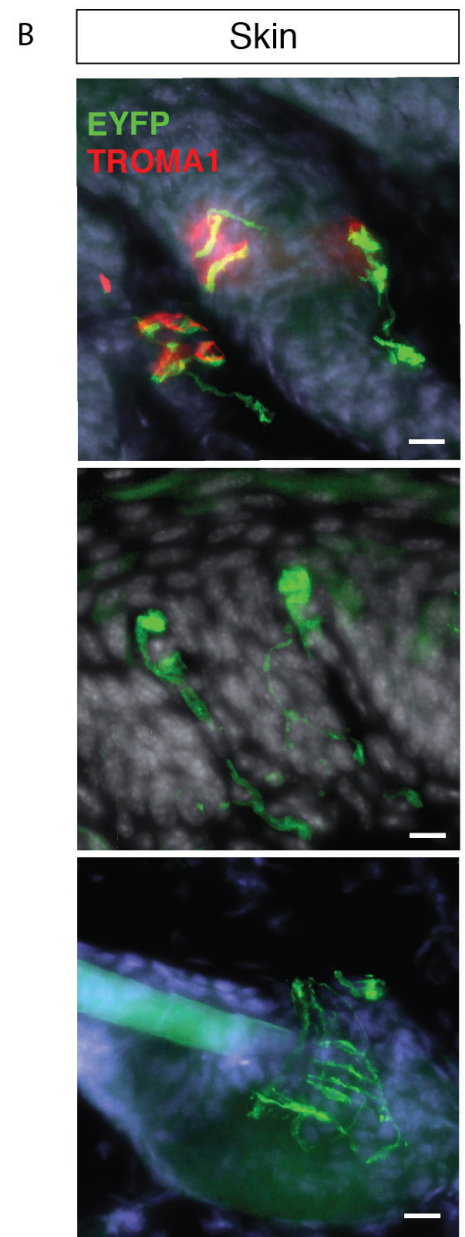
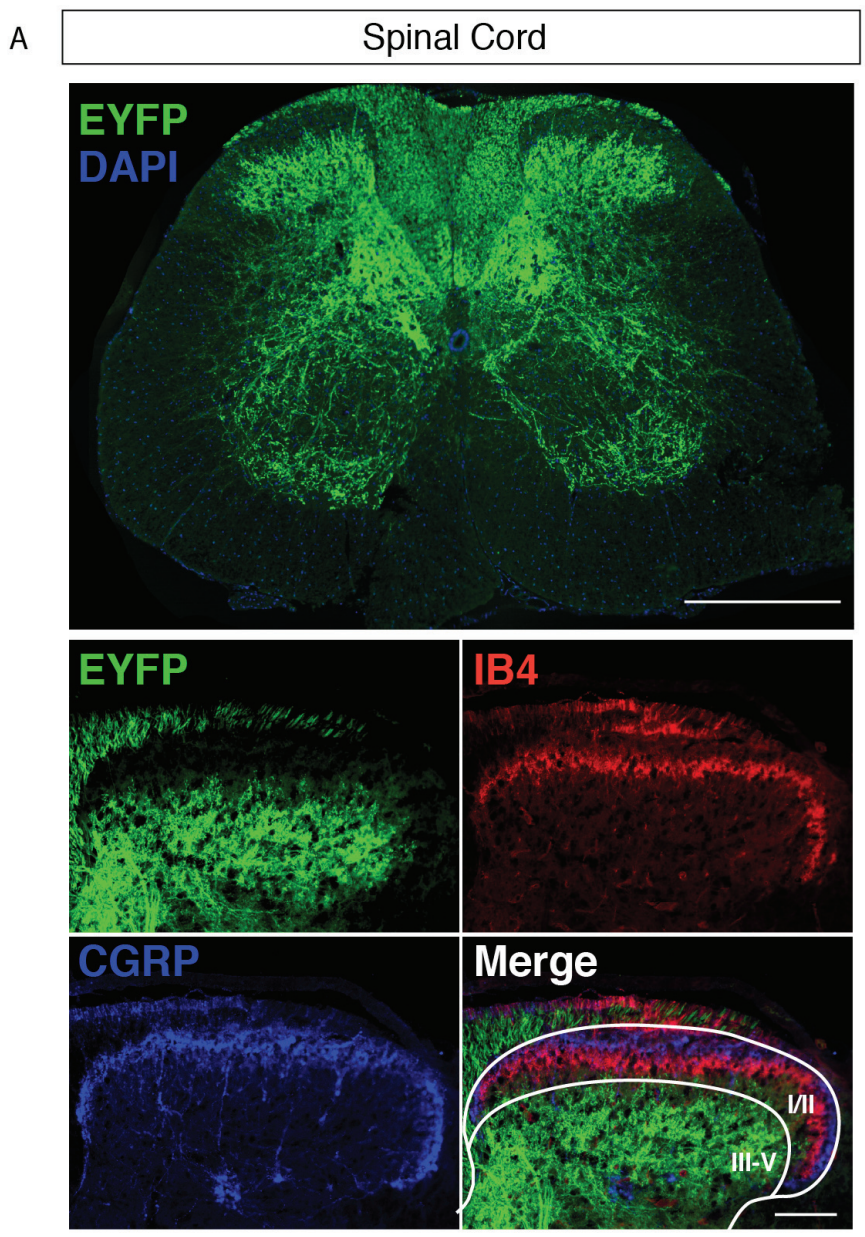
884 ipsilateral on post-operative day 7 (POD7) but not the contralateral paw. ( $n = 7$  mice/group);  
885 Two-factor LME, Tukey's post-hoc test. Paw:  $F_{(1,18)} = 8.27$ ,  $p = 0.01$ , Timepoint:  
886  $F_{(1,18)} = 11.92$ ,  $p = 0.003$ , Paw x Timepoint:  $F_{(1,18)} = 13.99$ ,  $p = 0.002$ , Post-hoc:  $**p < 0.01$ .  
887 **(B)**, The total number of light-evoked responses is not significantly different between the  
888 ipsilateral and contralateral paws on POD7. (Three-factor LME, Paw:  $F_{(1,90)} = 18.08$ ,  
889  $p = 0.0001$ , Timepoint:  $F_{(1,90)} = 7.16$ ,  $p = 0.009$ , Intensity:  $F_{(3,90)} = 32.45$ ,  $p < 0.0001$ , Paw x  
890 Timepoint:  $F_{(1,90)} = 0.28$ ,  $p = 0.60$ , Paw x Intensity:  $F_{(3,90)} = 2.10$ ,  $p = 0.11$ , Timepoint x  
891 Intensity:  $F_{(3,90)} = 1.59$ ,  $p = 0.20$ , Paw x Timepoint x Intensity:  $F_{(3,90)} = 1.43$ ,  $p = 0.24$ ). **(C)**,  
892 The number of reflexive responses is not different between ipsilateral and contralateral paws  
893 on POD7 (Three-factor LME, Paw:  $F_{(1,90)} = 18.24$ ,  $p < 0.0001$ , Timepoint:  $F_{(1,90)} = 7.32$ ,  
894  $p = 0.008$ , Intensity:  $F_{(3,90)} = 32.14$ ,  $p < 0.0001$ , Paw x Timepoint:  $F_{(1,90)} = 0.31$ ,  $p = 0.58$ , Paw x  
895 Intensity:  $F_{(3,90)} = 2.12$ ,  $p = 0.10$ , Timepoint x Intensity:  $F_{(3,90)} = 1.61$ ,  $p = 0.19$ , Paw x  
896 Timepoint x Intensity:  $F_{(3,90)} = 1.50$ ,  $p = 0.22$ ). **(D)** The number of affective-motivational  
897 responses is not different between ipsilateral and contralateral paws on POD7 (Three-factor  
898 LME, Paw:  $F_{(1,90)} = 0.09$ ,  $p = 0.77$ , Timepoint:  $F_{(1,90)} = 0.0$ ,  $p = 1.00$ , Intensity:  $F_{(3,90)} = 5.71$ ,  
899  $p = 0.001$ , Paw x Timepoint:  $F_{(1,90)} = 0.08$ ,  $p = 0.77$ , Paw x Intensity:  $F_{(3,90)} = 0.60$ ,  $p = 0.61$ ,  
900 Timepoint x Intensity:  $F_{(3,90)} = 0.29$ ,  $p = 0.83$ , Paw x Timepoint x Intensity:  $F_{(3,90)} = 0.26$ ,  $p =$   
901  $0.85$ ). **(E-F)**, Ipsilateral stimulation on POD7 did not produce more aversion compared to  
902 contralateral stimulation in a modified RT-PEA assay. One-Factor LME, E, Stage:  $F_{(1,12)} =$   
903  $0.98$ ,  $p = 0.40$ . F, Stage:  $F_{(2,12)} = 1.06$ ,  $p = 0.38$ ). All plots represented as mean  $\pm$  SEM.  
904



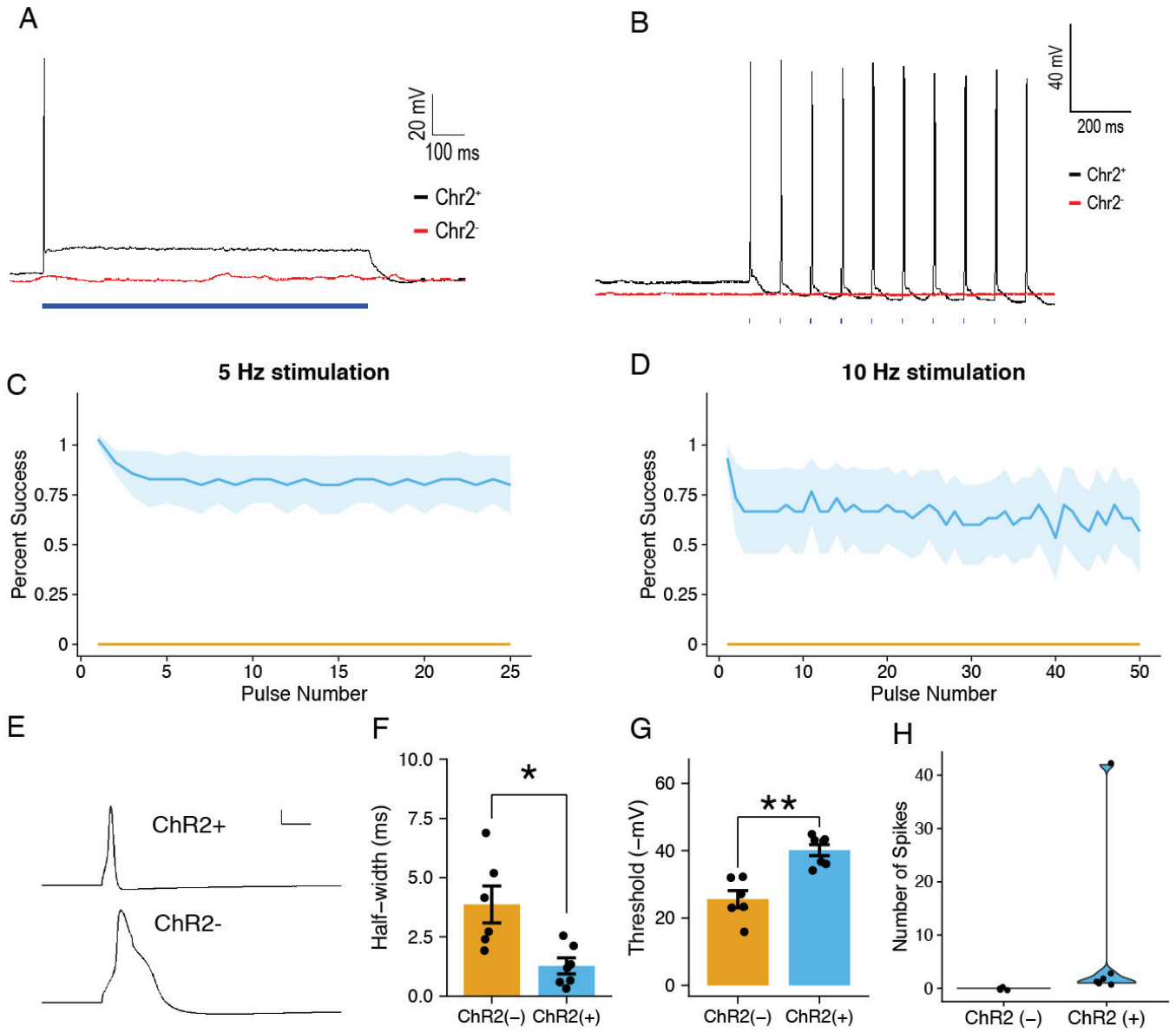


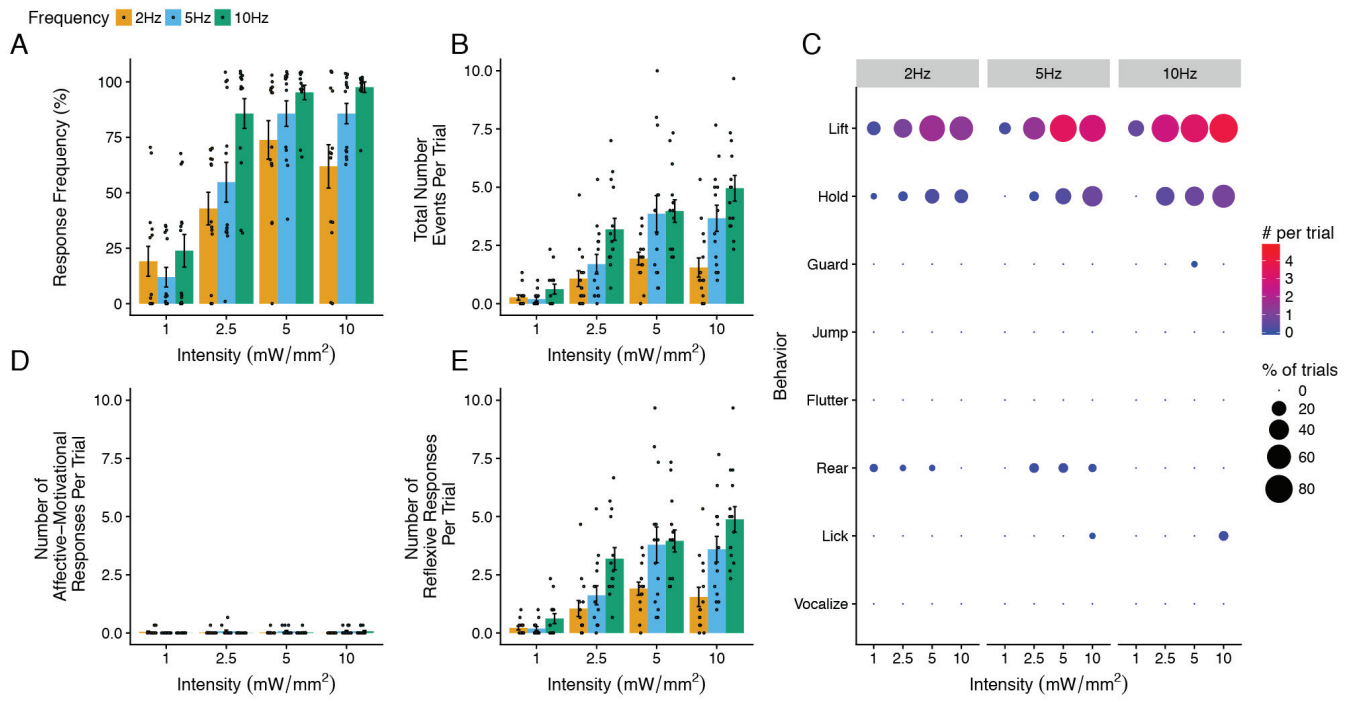




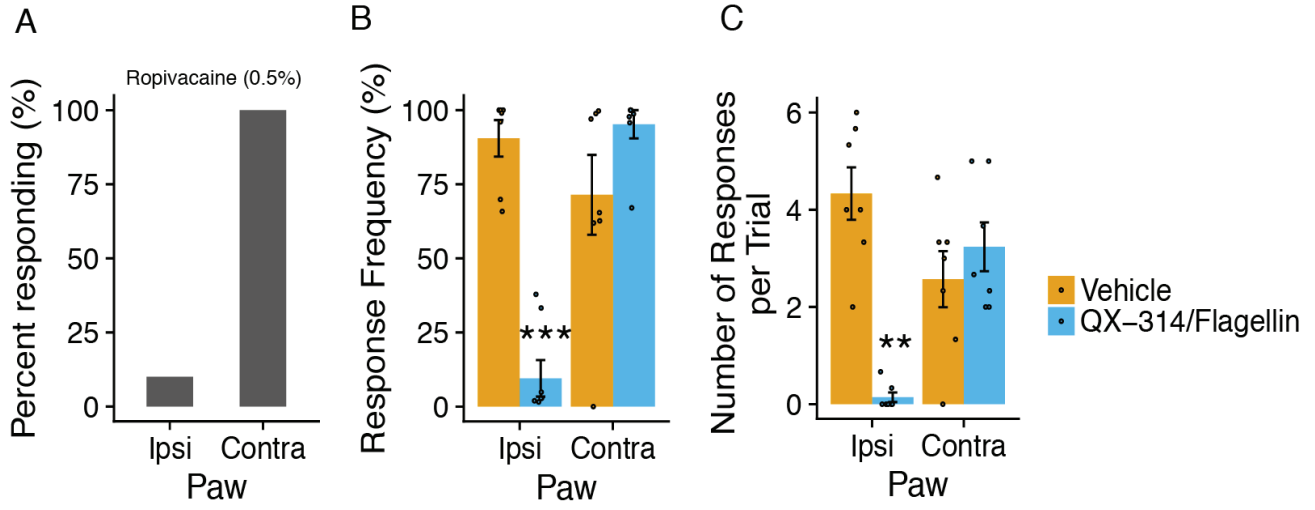












Genotype ■ Vglut1-ChR2 ■ Nav1.8-ChR2

